Critical functions and key interactions mediated by the RNase E scaffolding domain in *Pseudomonas aeruginosa*

Sandra Amandine Marie Geslain, Stéphane Hausmann, Johan Geiser, George Edward Allen, Diego Gonzalez and Martina Valentini*

Department of Microbiology and Molecular Medicine, CMU, Faculty of Medicine, University of Geneva, Geneva, Switzerland.

* To whom correspondence should be addressed. e-mail: Martina.Valentini@unige.ch

Abstract

The RNA degradosome, a multi-protein complex regulating mRNA in bacteria, assembles on the RNase E C-terminal domain (CTD) in Pseudomonadota (Proteobacteria) via short linear motifs (SLiMs). The composition of the *Pseudomonas aeruginosa* RNA degradosome is largely unknown, and its RNase E CTD shows limited similarity to those in models like *Escherichia coli* or *Caulobacter crescentus*. Our study characterizes the function of conserved SLiMs in *P. aeruginosa* RNase E, including a duplicated sequence termed the "REER-repeats" region. This region, along with AR1 and AR4 SLiMs, mediates RNA binding and localizes the degradosome in subcellular foci. Pull-down and bacterial two-hybrid assays identified PNPase and RhlB as interacting proteins, with direct interactions confirmed via protein binding assays. The NDPR and AR1 SLiMs mediate these interactions, respectively. Transcriptome analyses and phenotypic assays of RNase E CTD mutants revealed growth defects in specific conditions and virulence defects, revealing the importance of RNase E CTD RNA binding and RNA degradosome scaffolding for *P. aeruginosa* adaptability.

Author Summary

In this study, we investigate the RNA degradosome in *Pseudomonas aeruginosa*, a bacterium known for causing multiple types of human infections and for its multi-drug resistance. The RNA degradosome is a crucial multi-protein complex that regulates RNA levels, helping bacteria to rapidly adapt to various environments. We identified the key components of this complex in *P. aeruginosa* and mapped their interactions. Our findings also reveal that interaction between this complex and RNA is important for bacterial growth, particularly in cold conditions and during infection. We finally compare our findings with the RNA degradosome in other species, noting significant evolutionary convergence and unique characteristics in *P. aeruginosa*.

Our research sheds light on the complex mechanisms bacteria use to manage RNA and adapt to their surroundings, which could eventually inform new strategies to combat bacterial infections and resistance.

Introduction

In bacteria, the processing and degradation of mRNAs is primarily orchestrated by the RNA degradosome, a multi-enzyme complex that includes ribonucleases, RNA helicases, and various other proteins [1-5]. The RNA degradosome plays a crucial role in enabling bacteria to rapidly adapt to changing environmental conditions by swiftly modifying mRNA levels and broadly regulating gene expression [6, 7].

Most of our knowledge on the RNA degradosome derives from studies in *Escherichia coli*, where the RNase E endonuclease serves as the central component [8-11]. While the catalytic activity of *E. coli* RNase E resides in its N-terminal domain (NTD, amino acids 1-529), the C-terminal domain (CTD, amino acids 530-1061), or scaffolding domain, is intrinsically disordered and contains short linear motifs (SLiMs) of 10 to 40 amino acids to which the other RNA degradosome components bind [11, 12]. Core *E. coli* RNA degradosome components, namely the polyribonucleotide phosphorylase PNPase [13], the RNA helicase RhlB [14], and the glycolytic enzyme enolase [15], interact with RNase E in semi-stoichiometric ratios via the PBS (PNPase binding site), HBS (helicase binding site) and EBS (enolase binding cite) SLiM, respectively [16, 17]. The *E. coli* RNase E CTD also includes an amphipathic helix, called membrane targeting sequence or MTS, which tethers the entire complex to the inner membrane, and two RNA-binding SLiMs, AR1 (named also RBD) and AR2, which mediate contact with translating ribosomes, small non-coding RNAs and mRNAs [12, 18-21]. Additional proteins, such as RraA [22, 23], RraB [24], CsdA [25], Ppk [26], MinD [27, 28], and Hfq [29], can interact with *E. coli* RNase E in sub-stochiometric ratios or under non-standard conditions of growth (reviewed in [30]). Of importance, the RNase E NTD is essential for *E. coli* growth and rRNA processing [31], whereas deletion of the CTD is not lethal and alters mRNA levels without affecting rRNAs [19, 32-34]. This highlights the dual role of RNase E, with the NTD being crucial overall cell maintenance, and the CTD regulating specific RNA substrates through the assembly of the RNA degradosome.

RNase E orthologs are present in approximately 49% of sequenced bacterial genomes, and nearly all Pseudomonadota (formerly called Proteobacteria) encode at least one RNase E ortholog, with the notable exception of most *Campylobacter* and *Helicobacter* species [5, 30]. The RNase E NTD is remarkably conserved across most species, while the CTD varies considerably in sequence, length, and SLiMs composition, even between species belonging to the same order [30]. SLiMs variability is thought to drive the diversity of RNase E interacting partners, and therefore RNA degradosome composition, among bacterial species. For instance, in *Caulobacter crescentus,* RNase E interacts with PNPase, RhlB, RNase D, and the Krebs cycle enzyme aconitase [35, 36]. In *Anabaena* sp. strain PCC 7120, RNase E partners with PNPase, enolase, the RNA helicase CrhB, and RNase II [37-39], while in *Pseudomonas syringae* LZ4W, only RNase R and the RNA helicase RhlE were found to co-purify with RNase E in pull-down assays [40]. Similarly, in *Rhodobacter capsulatus*, purification of the RNA

degradosome complex via glycerol-gradient centrifugation of cell extracts revealed the presence of RNase E, two unnamed RNA helicases, the Rho transcription termination factor, and two unidentified proteins of 47 and 36 kDa, with only low amounts of PNPase present in the purified fractions [41].

In these examples, the SLiMs mediating protein-protein interactions were not always characterized. Besides, even when the interaction of RNase E with a certain protein partner is conserved across several species, such as the RNase E-PNPase and RNase E-RhlB interactions, the SLiMs involved in the binding show little sequence identity [30, 36, 37, 42-44]. Therefore, predicting RNA degradosome composition based solely on the RNase E CTD sequence does not seem possible. Experimental characterization of the SLIMs across different bacterial species and their impact on the RNA degradosome composition and function is therefore essential, providing insights into novel regulatory mechanisms that enable bacteria to thrive under stress and adapt to diverse environments.

Little is known about the RNA degradosome composition of the opportunistic pathogen *Pseudomonas aeruginosa*, which is a leading cause of nosocomial infections worldwide largely due to its remarkable adaptability to different environments and resistance to antibiotics [45-53]. A recent study has revealed that the φKZ bacteriophage protein Dip interacts with *P. aeruginosa* RNase E, leading to its co-elution with RNase E but also with PNPase, the PA0428 RNA helicase, and several other proteins in pull-down assays [54]. Therefore, the RNA degradosome of *P. aeruginosa* was assumed to be composed of these proteins [5], although their interaction with RNase E has neither been confirmed nor mapped. Our laboratory has characterized the PA0428 RNA helicase, named RhlE2, confirming an RNA-dependent interaction with RNase E and identifying the RhlE2 C-terminal region as necessary and sufficient for this binding [55, 56]. However, the specific RNase E interaction site remained unmapped.

In this study, we characterize the SLiMs within the CTD of *P. aeruginosa* RNase E, identifying those involved in RNA binding (AR1, AR4, and REER-repeats) as well as those mediating interactions with core RNA degradosome components, which we determine to be PNPase and the RNA helicase RhlB (NDPR and AR1, respectively). We also show that RhlE2 interacts with the RNase E NTD in pull-down assays. Protein-protein interactions were probed with multiple experimental approaches, including an analysis of the subcellular localization dynamics of the complex. Additionally, we performed transcriptomic and phenotypic analyses of RNase E CTD mutant strains, revealing the critical role of RNA degradosome complex scaffolding in bacterial virulence, adaptation to cold temperatures and to pH fluctuations.

The ability of *P. aeruginosa* to cause disease is intrinsically linked to a sophisticated gene regulatory network that facilitates bacterial survival and virulence. Within this network, the role of post-transcriptional gene regulation remains only partially explored [57, 58]. By uncovering the composition and functional dynamics of the RNA degradosome in *P. aeruginosa*, our study not only advances the understanding of the molecular mechanisms driving bacterial environmental adaptation but also reveals potential novel drug targets, which could be crucial in the fight against antibiotic-resistant infections.

Results

Pa RNase E harbours several uncharacterised SLiMs conserved within the Pseudomonadales

P. aeruginosa RNase E (Pa RNase E) consists of an NTD (amino acids 1-529) that shares high sequence identity (70%) and similarity (90%) with the NTD of *E. coli* RNase E (Ec RNase E), and a CTD (amino acids 530-1057) that shows only 25% identity and 37% similarity with the CTD of Ec RNase E (Fig. S1). Aït-Bara and colleagues (2015) identified seven putative SLiMs on the Pa RNase E CTD (MTS, AR4, REE, M29, AR1, M20 and NDPR) [59], which are shown in comparison to the Ec RNase E in Fig. S2A. Of note, the MTS is the only SLIM of Pa RNase E CTD with a propensity to form a secondary structure while in Ec RNase E, the helicase, enolase, and PNPase binding sites also exhibited this feature (Fig. 1 and [12]).

To refine the prediction of Pa RNase E SLiMs, we performed a multiple sequence alignment of 5000 Pseudomonas RNase E orthologs and identified conserved motifs (Fig. S3). Several highly conserved regions of the CTD overlap with the SLiMs previously identified, with the notable presence of additional conserved residues located immediately adjacent to these SLiMs (Fig S2/S3). Based on these data, we redefined the boundaries of the SLiMs to integrate these conserved residues (Fig. 1B, see Fig. S2A for former SLiMs). Upon manual inspection of the CTD sequence, we also observed a large duplicated sequence (residues 635-667 and 682-714) within the CTD region containing the REE and motif 29 SLiMs. Since motif 29 is characterised by the conserved motif REERQPR, we have merged the two SLiMs and renamed the entire region (residues 614-729) as the "REER-repeats" region (Fig. 1B). The number of REER repeats varies across Pseudomonas species: *P. aeruginosa* strains typically harbour 13 RE[ED]R repeats, while the environmental *P. fluorescens*, *P. protegens*, *P. stutzeri*, and *P. syringae* groups show a distribution of repeats peaking around 8-10. Exception is *P. putida*, which exhibits a high frequency of 20-23 RE[ED]R repeats (Fig. S2B). This variability suggests a high frequency of indels occurring within the REER-repeats region.

Overall, our in-silico analyses of Pa RNase E CTD sequence redefined the number and length of the putative Pa RNase E SLiMs, highlighting a potential functional significance of the REER-repeats region in Pseudomonas species, and suggesting different RNA degradosome complex dynamics in *P. aeruginosa* as compared to *E. coli*.

The REER-repeats, AR1 and AR4 SLiMs mediate RNase E CTD RNA binding and foci formation

Previous works in *E. coli* identified arginine-rich SLiMs as RNA-binding motifs [21, 60]. We therefore hypothesized that the *P. aeruginosa* AR1 and AR4 SLiMs, along with the newly identified REER-repeat region, might be involved in RNA binding. To test this hypothesis, we conducted electrophoretic mobility shift assays (EMSA) to examine the binding of purified RNase E CTD proteins to an in vitro synthesized RNA derived from the *malEF* intergenic region (for details, see methods). We tested wild-type (WT) CTD and mutated variants where arginine residues in AR1, AR4, or the REER-repeats were

150 replaced with alanine (named AR1mut, AR4mut, and REERmut, respectively). Qualitative analysis of
151 the EMSA showed that the WT, AR1mut, and AR4mut variants bound RNA with similar efficiency, as
152 indicated by comparable gel shift patterns (Fig. S4A). However, the REERmut variant exhibited slightly
153 reduced RNA binding, evidenced by a delayed shift as compared to the former proteins (Fig. S4B and
154 2A). The combination of AR1 and AR4 mutations resulted in an impaired RNA binding which was
155 further exacerbated when the REER mutation was also introduced: no observable shift in the RNA was
156 detected when incubated with the protein variant carrying mutations in all three SLiMs, even at an
157 RNA-to-protein ratio of 1:80 (Fig. 2A). Together, these results highlight the functional redundancy of
158 the AR1, AR4, and REER-repeat SLiMs in RNA binding, as a significant defect in RNA binding is
159 observed only when all these SLiMs are simultaneously disrupted.
160 One notable characteristic of the RNA degradosome is its tendency to form highly dynamic subcellular
161 foci, also referred to as "clusters," "puncta," or "helical structures" [28, 61]. These foci rapidly
162 disassemble upon rifampicin treatment, suggesting their formation is RNA-dependent [61, 62]. In *E.*
163 *coli*, these foci are membrane-anchored via the MTS SLiM, whereas in *C. crescentus* they remain
164 cytoplasmic, driven by liquid-liquid phase separation [62, 63]. To investigate the subcellular localisation
165 of Pa RNase E, we constructed *P. aeruginosa* PAO1 strains expressing msfGFP-tagged Pa RNase E, Pa
166 RNase E^{1-588}, or Pa RNase E^{1-529} from the native *rne* locus. The two RNase E truncations were designed
167 based on our in-silico analysis of Pa RNase E SLiMs, assuming that they would lack the capacity to
168 assemble the RNA degradosome. The key difference between RNase E^{1-588} and RNase E^{1-529} lies in the
169 presence of the MTS (Fig. 1B). Visualization using epifluorescence microscopy revealed that RNase E-
170 msfGFP forms foci concentrated near the cell edge (Fig 2B). Both CTD truncation mutants showed
171 impairment in foci assembly, but while the RNase E^{1-588}-msfGFP protein localises uniformly around the
172 edge of the bacteria, the RNase E^{1-529}-msfGFP mutant protein additionally fails to localise near the
173 membrane, consistent with the role of the MTS in membrane anchoring (Fig. 2B).
174 Exposure of Pa RNase E-msfGFP expressing cells to high levels of rifampicin (100 µg/ml) led to the
175 dissipation of these foci, resulting in a smoother distribution of the signal along the cell periphery, which
176 phenocopies the localization of the RNase E^{1-588}-msfGFP strain (Fig. 2D). Quantitative analysis
177 confirmed a significant reduction in signal intensity variance upon rifampicin treatment as compared to
178 the control (DMSO-only), indicating foci dissipation, while the average signal intensity remained
179 constant, ruling out RNase E- msfGFP proteolysis (Fig. 2E-F, Fig. S4F).
180 To further verify that Pa RNase E-msfGFP foci formation depends on CTD-mediated RNA binding, we
181 constructed *P. aeruginosa* strains with chromosomally msfGFP-tagged RNase E variants mutated in
182 AR1, AR4, and REER-repeats SLiMs, individually and in combination, as done previously for the
183 EMSA. Visualisation of these variants showed a clear correlation between CTD-mediated RNA binding
184 and foci formation. Specifically, the RNase E AR1+AR4mut-msfGFP showed less distinct foci and
185 lower signal variance compared to RNase E-msfGFP and single AR1 or AR4 mutants (Fig. 2B-C). The
186 RNase E REERmut-msfGFP also had diffuse foci and lower variance, while the RNase E

187 AR1+AR4+REERmut-msfGFP, with abolished RNA binding, displayed the most severe disruption,
188 with nearly complete loss of foci and a very narrow signal intensity distribution (Fig. 2B-C and Fig.
189 S4F). Similar patterns were observed with CTD truncations containing different combinations of RNA-
190 binding SLiMs, ruling out the possibility that this foci dissipation is caused by the changed in the charge
191 of the CTD conferred by the mutations (Fig. S4E).
192 Of note, we noticed an increased signal intensity in all the msfGFP-tagged RNase E mutants tested as
193 compared to the RNase E-msfGFP (Fig. S4C). Since all constructs are expressed at the native locus,
194 this could likely reflect higher RNase E protein levels, which suggests that CTD-mediated RNA binding
195 might be necessary for RNase E autoregulation [64]. To confirm this, we performed a Western Blot on
196 strains expressing several Strep-tagged RNase E mutants and could indeed observe that RNase E protein
197 levels are increased upon deletion of the CTD or introduction of AR1+AR4+REERmut (Fig. S4D).
198 Overall, we conclude that in *P. aeruginosa*, the organisation of the RNA degradosome complex into
199 visualisable foci is dependent on the RNase E CTD-mediated RNA binding and suggest that this
200 interaction not only organizes the localisation of the RNA degradosome but could also influence the
201 regulatory activity of RNase E.
202
203 **Identification of proteins binding to RNase E scaffold domain**
204 In *P. aeruginosa*, the RNA degradosome was proposed to include the RhlE2 RNA helicase (called
205 DeaD), PNPase, and other associated proteins [54, 55]. However, the direct nature of these interactions
206 and the specific interaction sites have not been demonstrated nor mapped. Additionally, RNase R was
207 also suggested to be a *P. aeruginosa* RNA degradosome component, as it is in *P. syringae* LZ4W [30,
208 40]. To test these hypotheses and identify Pa RNase E CTD interacting proteins, we performed a pull-
209 down assay using *P. aeruginosa* strains expressing C-terminal Strep II-tagged full-length RNase E
210 (RNase E^{1-1057}-Strep) or an RNase E truncation missing the entire CTD (RNase E^{1-529}-STREP). As an
211 additional control, the assay was also performed with the *P. aeruginosa* PAO1 wild-type (WT) to discard
212 proteins interacting nonspecifically with the Strep-Tactin magnetic beads (Fig. 3A-B).
213 Eluates of the pull-down experiment were first analysed by silver staining (Fig S5). The RNase E^{1-1057}-
214 Strep eluate revealed a high molecular weight band corresponding to RNase E, along with additional
215 bands absent in the untagged and RNase E^{1-529}-Strep samples. These bands likely represent components
216 of the RNA degradosome or cleaved RNase E^{1-1057}-Strep intermediates, as RNase E is known to be
217 prone to cleavage [42, 65]. Mass spectrometry (LC-MS/MS) analysis identified a total of 115 proteins
218 present in both duplicates of the RNase E^{1-1057}-Strep eluates. 13 proteins (including RNase E) were
219 enriched by at least 5.5-fold as compared with the untagged sample (Fig 3A). This stringent threshold
220 was chosen since core components of the RNA degradosome should be abundantly associated to RNase
221 E. Of these 12 putative partners, 5 (PNPase, GdhB, ArcB, RhlB and RpoB) were completely absent
222 from both RNase E^{1-529}-Strep duplicates and 2, namely RpoC and RplL, were absent from one replicate
223 and present in the second replicate with a peptide count of 2. We selected for further study the first 5

224 proteins, which were considered the most promising RNA degradosome candidates as their interaction
225 with Pa RNase E seemed fully dependent on the CTD.
226 It is worth noting that the RhlE2 RNA helicase was, as expected [54, 55], among the proteins enriched
227 in the RNase E^{1-1057}-Strep eluate as compared to the untagged control, but surprisingly it was equally
228 enriched in the RNase E^{1-529}-Strep eluate condition (Fig 1C), indicating that this interaction occurs via
229 RNase E NTD and not via the CTD.
230
231 **RNase E direct interaction with PNPase and RhlB occur via the NDPR and AR1 SLiMs,**
232 **respectively**
233 The interaction between RNase E and the 5 candidates was first verified using an adenylate-cyclase-
234 based bacterial two-hybrid (BTH) assay [66]. Co-expression of T25-PNPase and T25-RhlB with T18-
235 RNase E resulted in red colonies on MacConkey agar and a significant increase of β-galactosidase
236 activity compared to empty vector controls (11-fold or 5-fold increase, respectively), confirming their
237 interaction (Fig S6A, Fig. 3C). Co-expression of T25-ArcB with T18-RNase E also resulted in a
238 significant increase in β-galactosidase activity (5-fold) compared to the negative control (Fig. 3C, Fig.
239 S6A). To identify the SLiMs mediating the observed interactions, we generated seven CTD truncations
240 of RNase E, each lacking an additional SLiM as compared with the longer version. Testing these
241 truncations for their capacity to interact with PNPase revealed that only T18-RNase E^{1-1025} showed β-
242 galactosidase activity similar to those of T18-RNase E^{1-1057} upon co-expression with T25-PNPase (Fig.
243 3D, Fig. S6B). In contrast, all shorter T18-RNase E CTD truncations except T18-RNase E^{1-529}, and also
244 T18-RNase $E^{940-1057}$, exhibited a significant increase of β-galactosidase activity as compared with the
245 negative controls but lower than T18-RNase E^{1-1057} (Fig. 3D, Fig. S6B). Overall, this suggests that
246 PNPase interaction with RNase E relies on two distinct sites of RNase E CTD: residues 529-588 and
247 940-1057. Co-expression of the T18-RNase E CTD truncations with T25-RhlB revealed that the
248 protein-protein interaction is mediated by residues 733-793: no significant interaction could be seen
249 between T25-RhlB and T18-RNase E^{1-733}, although T25-RhlB could interact with T18-RNase E^{1-793} (and
250 every longer CTD truncation) or with T18-RNase $E^{733-793}$ about as strongly as with T18-RNase E^{1-1057}
251 (Fig. 3E, Fig. S6C). Of note, neither T18-RNase $E^{733-761}$ nor T18-RNase $E^{762-793}$ were able to restore β-
252 galactosidase activity above negative control levels when co-expressed with T25-RhlB (Fig. 3E),
253 suggesting that the entire AR1 SLiM, as defined in Fig 1B, is necessary for interaction with RhlB.
254 Surprisingly, all T18-RNase E CTD truncations, except T18-RNase E^{1-529}, significantly interact with
255 T25-ArcB, suggesting a complex binding that is dependent on residues 529-588 (Fig. 3F, Fig. S6D). Of
256 note, these residues only contain the MTS SLiM, which is presumably involved in membrane binding.
257 Building on the bacterial two-hybrid assays results, we successively employed affinity chromatography
258 with purified proteins to investigate direct binding, minimizing the influence of other protein partners
259 or RNA. Fusion proteins containing a C-terminal 3xFlag tagged RNase E^{1-529}, RNase $E^{572-1057}$ (CTD
260 with no MTS) or RNase E^{1-1057} were purified and immobilized on anti-Flag magnetic beads. After

extensive washing, the beads were mixed with either purified PNPase, RhlB, or ArcB proteins. Analysis of the bound and free fraction was performed by SDS-page (Fig. 4).

PNPase was retained on beads containing Flag-RNase $E^{572-1057}$, but not on beads alone or containing Flag-RNase E^{1-529} (Fig. 4A), indicating that the RNase E CTD is sufficient for direct interaction with PNPase. Point mutations within the NDPR SLiM (Flag-RNase $E^{572-1057}$_NDPRmut) confirmed that this SLiM is necessary for this interaction, as suggested by the observed interaction between T18-RNase $E^{940-1057}$ truncation and T25-PNPase in the BTH assay (Fig. 4A).

Similarly, RhlB was retained on Flag-RNase $E^{572-1057}$ but not on Flag-RNase E^{1-529} and point mutations in the AR1 SLiM (Flag-RNase $E^{572-1057}$–AR1mut) showed that this region is crucial for RhlB binding (Fig. 4B).

Contrary to PNPase or RhlB, ArcB was not retained on beads containing Flag-RNase E^{1-1057} under the tested conditions, suggesting an indirect type of interaction (data not shown). To summarize, these experiments clearly establish PNPase and RhlB as core components of *P. aeruginosa* RNA degradosome and demonstrate that the AR1 and NDPR SLiMs are essential for their direct interactions with RNase E.

PNPase and RhlB are dependent on their physical interaction with RNase E for colocalising in RNA degradosome foci.

Given the foci localization of RNase E, we assessed PNPase and RhlB colocalization with RNase E by using *P. aeruginosa* strains carrying *rne::mCherry* and either *pnp::msfGFP* or *rhl::msfGFP* chromosomal fusions. As expected, both PNPase-msfGFP and RhlB-msfGFP formed foci near the membrane and co-localized with RNase E-mCherry in live cells (Fig. 5A). Overlap coefficients between the two fluorescence channels were consistently over 0.9, while Pearson's coefficients were slightly lower (0.880 for PNPase and 0.773 for RhlB), likely due to differences in signal intensity. Of note, strains expressing any of these chromosomal fusion proteins grow identically to the WT strain at 37°C, suggesting that all the fusion proteins are functional (Figure S7A). We also assessed the subcellular localisation of ArcB-msfGFP and observed a smooth distribution rather than foci, which suggests that the interaction between RNase E and ArcB is likely transient, with ArcB not being a core component of the complex (data not shown).

To further corroborate the need for specific RNase E domains in these interactions, we examined the localization of PNPase-msfGFP and RhlB-msfGFP in strains expressing RNase E^{1-1057} (WT), RNase E^{1-529} (*rne529*), RNase E^{AR1mut} (*rne*$AR1^{mut}$), or RNase $E^{NDPRmut}$ (*rne*$NDPR^{mut}$). Both PNPase-msfGFP and RhlB-msfGFP displayed diffuse cytosolic localization in the *rne529* strain compared to the WT strain (Fig. 5B). In the *rne*$NDPR^{mut}$ strain, PNPase-msfGFP showed a diffuse cytosolic distribution, while RhlB-msfGFP was diffuse in the *rne*$AR1^{mut}$ strain. However, NDPR or AR1 mutations did not prevent RhlB or PNPase from being recruited into RNase E foci, respectively, indicating that both proteins can be independently recruited into RNase E-driven foci (Fig. 5B). We also confirmed that RNase E

298 NDPRmut-msfGFP forms foci, ruling out the possibility that the loss of PNPase foci in the *rne*NDPR^{mut}
299 strain is due to impairment of RNase E-driven foci formation (Figure S7B). These findings confirm the
300 in vivo interaction of Pa PNPase and Pa RhlB with the NDPR and AR1 SLiMs, respectively, and
301 demonstrate that these interactions are crucial for their near-membrane foci localization.
302
303
304 **Phenotypic changes associated with partial or complete deletion of RNase E CTD**
305 To investigate the biological importance of RNase E CTD-mediated complex scaffolding in *P.*
306 *aeruginosa*, we performed some phenotypic assays using the *rne529* and *rne588* strains, as well as
307 strains bearing the AR1 mutation (*rne*AR1^{mut}), NDPR mutation (*rne*NDPR^{mut}), or AR1+AR4+REER
308 mutation (*rne*AR1+AR4+REER^{mut}), abolishing RhlB binding, PNPase binding, or CTD-mediated RNA
309 binding, respectively.
310 At 37°C in liquid culture, only the *rne529, rne588* and *rne*AR1+AR4+REER^{mut} strains exhibited a slight
311 but consistent growth delay (Fig. 6B). On solid media at 37°C, the *rne529* and *rne*AR1+AR4+REER^{mut}
312 strains also displayed reduced colony size, confirming the growth delay (Fig. 6A, top panel). To verify
313 that the growth delay was caused by truncations/mutations introduced in the *rne* gene, we electroporated
314 the WT or the two mutant strains with an inducible vector allowing in trans expression of RNase E,
315 RNase E-msfGFP, or RNase E-mCherry. Cultivation of the strains at 37°C in liquid culture revealed
316 that expression of either native or fluorescently-tagged RNase E could restore identical growth levels
317 compared to the electroporated WT strain, additionally confirming that the fluorescently-tagged RNase
318 E protein is fully functional (Fig S10).
319 Unexpectedly, when cultured on solid media at 16°C, the *rne588* strain showed impaired growth, while
320 the growth defects of the *rne529* and *rne*AR1+AR4+REER^{mut} strains became more pronounced, with
321 *rne529* barely growing (Fig. 6A, upper middle panel). Since the *rne*AR1^{mut} and the *rne*NDPR^{mut} strains
322 exhibited no significant differences compared to the WT, these results indicate that the cold sensitivity
323 of the *rne588* strain can be attributed to the loss of RNase E CTD RNA binding. Moreover, the severe
324 growth defect observed in the *rne529* mutant indicates that additional delocalisation of RNase E from
325 the membrane exacerbates the cold sensitivity caused by deletion of RNase E RNA-binding SLiMs.
326 Besides low temperature, we also tested sensitivity to low or high pH (Fig. 6A, lower panels): while
327 growth at pH≃9.5 is similar between the different strains, deletion of the CTD (*rne529* and *rne588*)
328 impairs growth at pH≃5.5, although the three CTD point mutant strains are mostly unaffected. This
329 suggests that, although loss of interaction with PNPase or RhlB separately does not seem to impair
330 growth, the combined loss of RNase E protein-protein and protein-RNA interactions results in a growth
331 defect under low pH conditions. Finally, we assessed whether the RNase E CTD mutants might be
332 impaired in virulence using *Galleria mellonella* larvae, a highly predictive infection model for studying
333 mammalian infection processes [67]. Infection with PAO1 WT, *rne*AR1^{mut} and *rne*NDPR^{mut} strains
334 resulted in 100% larval mortality within 20 hours post-injection (Fig 6C). In contrast, the larvae infected

335 with the *rne588* mutant exhibited 50% survival at this time point, while those infected with
336 *rne*AR1+AR4+REER^{mut} or *rne529* mutants showed 100% survival, with larval death occurring only
337 after 21 hours post-injection (Fig 6C). These results strongly indicate that the ability of *P. aeruginosa*
338 to infect a host is compromised when RNase E CTD-mediated RNA binding is disrupted. This
339 impairment is likely attributable to several contributing elements: reduced bacterial growth within the
340 host, deficiencies in virulence factor production, and a decreased ability to endure host immune
341 responses and host-related stresses.
342
343 **Effect of RNase E CTD on *P. aeruginosa* transcripts steady-state levels**
344 To better understand the phenotypes observed and evaluate the impact of RNase E CTD loss on *P.*
345 *aeruginosa* transcriptome, we conducted RNA-sequencing analysis on *P. aeruginosa* WT, *rne529* and
346 *rne588* mutant strains grown at 37°C until the late-exponential growth phase (OD_{600nm} of 1-1.2). Under
347 these conditions, the loss of the entire RNase E CTD in the *rne529* strain affected the steady-state levels
348 of 450 transcripts, with 183 downregulated and 267 upregulated (P-value < 0.05, fold change |FC| ≥ 2)
349 (Fig. 7A). In the *rne588* mutant, 417 transcripts were differentially expressed, with 194 downregulated
350 and 223 upregulated (P-value < 0.05, fold change |FC| ≥ 2) (Fig. 7B). Differential expression analysis
351 on reads mapping to predicted small RNA genes (sRNAs) identified 14 predicted sRNA genes with
352 significantly enriched reads in the *rne529* mutant and 5 in the *rne588* strain (Table S3 and Figure S).
353 A comparison of the *rne529* and *rne588* strains revealed that 164 mRNAs were consistently regulated
354 in both mutants (97 upregulated and 67 downregulated, see Figure 7C). Among the strongest commonly
355 downregulated genes were: the *pqsABCD* genes, involved in the synthesis of quorum-sensing signal
356 molecules alkylquinolones PQS (2-heptyl-3-hydroxy-4(1H)-quinolone) and HHQ (2-heptyl-4(1H)-
357 quinolone) and in virulence (with the entire *pqsE*, *pqsH* and *phnAB* PQS synthesis cluster being
358 downregulated in *rne529* strain) [68], the *phzA1B1* and *phzA2B2* phenazine biosynthesis genes, which
359 are important for synthesis of the toxic secondary metabolites phenazine and pyocyanin [69], and the
360 *agtABCD* gene cluster for 4-aminobutyrate (GABA) and 5-aminovalerate (AMV) uptake [70].
361 Surprisingly, the two strains exhibited more differences in mRNA levels than shared changes. In the
362 *rne588* strain, the mRNA levels corresponding to type 3 secretion system genes, which deliver toxins
363 to host cells [71], were consistently upregulated, while they did not vary significantly in the *rne529*
364 strain as compared to the WT (Fig 7D). On the other hand, ribosomal and many amino acid metabolism
365 genes (tryptophan, arginine, alanine, aspartate and glutamate) were downregulated only in the *rne529*
366 strain, which could correlate with the general growth defect observed (Fig. 7E and Table S4).
367 Considering the autoregulation of RNase E reported in *E. coli* and *C. crescentus* [64, 72], we quantified
368 reads mapping to the 5' untranslated region (UTR) of the *rne* gene (TSS determined in [73]) and
369 observed increases of 2 and 0.96 $\log_2$ folds in the *rne529* and *rne588* mutants, respectively, compared
370 to the WT (Fig. 7F). Similarly, we observed a 1.43 and 0.88 $\log_2$ fold increase in the transcript

371 corresponding to the NTD of RNase E in the *rne529* and *rne588* mutants, respectively (Fig. 7F), in
372 agreement with the observed increase in protein levels (Fig. S4C-D).
373 Finally, to assess RNA degradation efficiency in our strains, we analysed the 5' reads ends of sequenced
374 RNA fragments. As previously performed in other studies [56, 74], we calculated the ratio between the
375 number of loci with 5' ends present only in a mutant and not in the WT, over the sum of loci with 5'
376 read ends seen in both mutant and WT. We performed the analysis in the three genetic backgrounds
377 (WT, *rne529*, *rne588*) and for each replica independently to ensure consistency (see methods and Fig
378 S9). Despite the background of random fragmentation intrinsic to the sequencing protocol, a consistent
379 increase on the number of 5' ends in the *rne529* and *rne588* strains was observed as compared to the
380 WT (Fig. 7G), suggesting an accumulation of RNA degradation intermediates and an altered RNA
381 degradation in the RNase E truncated mutants.
382
383 **Discussion**
384
385 The composition and the functions of the RNA degradosome vary among bacterial species, likely
386 reflecting diverse lifestyles and niche adaptations [59]. Studying the variations of the RNA
387 degradosome composition in various bacterial species is therefore crucial for elucidating how bacteria
388 respond and adapt to different environmental conditions and sustain various types of stress. In this study,
389 we characterized the RNA degradosome of *P. aeruginosa*, a versatile opportunistic pathogen and widely
390 used model organism for bacterial pathogenesis and environmental adaptation.
391 In the first part of our study, we focused on the putative SLiMs within the CTD of *P. aeruginosa* RNase
392 E and assessed their contribution to RNA binding, as well as to binding the other core RNA
393 degradosome components, which we identified as RhlB and PNPase via pull-down assays (Fig. 8). A
394 notable feature of SLiMs is their poor sequence conservation, even when they mediate interactions with
395 the same protein partner. Our findings confirm this variability for both PNPase and RhlB interactions.
396 PNPase, a known partner of RNase E in several species, binds through SLiMs with significantly
397 different sequences across organisms. For instance, in *Anabaena* PCC7120, the interaction occurs via a
398 cyanobacterial SLiM having the conserved residues RRRRRRSSA [37], while in *E. coli* or *C.*
399 *crescentus*, the sequences are WQRPTFAFEGKGAAGGHTATHHASA [30] and
400 APPEKPRRGWWRR [43], respectively. Our pull-down assays and in vitro binding assays showed that
401 PNPase interacts with RNase E in *P. aeruginosa* via the NDPR SLiM, which has yet another distinct
402 sequence (TGRALNDPREKRRLQREAERLAREAAAAA). These sequence variations may reflect
403 species-specific interactions, as suggested by experimental work showing lack of heterologous
404 interactions between RNase E and PNPase of *E. coli* and *Pseudoalteromonas haloplanktis* [42]. Despite
405 sequence variability, the PNPase interacting SLiM is consistently located towards the end of the RNase
406 E CTD [30, 37, 43], suggesting convergent evolution in the positioning of the PNPase relative to other
407 RNA degradosome components and to RNase E catalytic domain.

408 Of note, a recent study on a *P. aeruginosa* mutant with a 50 bp deletion in the 3' end of the *rne* gene
409 revealed a hypervirulence phenotype, characterized by enhanced cytotoxicity and siderophore
410 production [75]. Based on *E. coli* RNA degradosome model, this phenotype was associated with a
411 possible impairment of PNPase binding to Pa RNase E or a different RNA degradosome activity [75].
412 Our data reveal that PNPase can interact with the RNase E^{1-1025} truncation (BTH assay), ruling out the
413 former hypothesis. However, we cannot exclude the possibility that this region might be involved in
414 interaction with a yet unknown partner.
415 Regarding RhlB, we show that in *P. aeruginosa*, this RNA helicase directly interacts with RNase E via
416 the AR1 SLiM (RPRRRSRGQRRRSNRRERQR). Mutation of AR1 disrupts not only the RhlB-RNase
417 E binding *in vitro*, but also RhlB subcellular localisation near the membrane and co-localization with
418 RNase E *in vivo*. Interestingly, in *E. coli* and other species the AR1 SLiM mediates RNA interaction
419 [30, 42]. In *P. aeruginosa*, AR1 also contributes to RNA-binding in addition to RhlB binding. Given
420 that in *E. coli,* a single arginine mutation within the HBS SLiM (R730A) is sufficient to disrupt RhlB
421 binding [76], it is possible that only one or a few arginine residues of the AR1 SLiM are involved in
422 interaction with RhlB, while the others mediate RNA binding. Further experiments are needed to
423 address this hypothesis and to understand the dynamics of the RhlB-RNA-RNase E complex in *P.*
424 *aeruginosa*. Moreover, it has been shown that the RNA-dependent ATPase and unwinding activity of
425 RhlB are stimulated by binding to RNase E [77]. Future studies will investigate whether it is also the
426 case in *P. aeruginosa*.
427 In contrast with the *E. coli* RNA degradosome, we did not find any evidence of an interaction between
428 RNase E and enolase or another metabolic enzyme in *P. aeruginosa* when the bacteria grow in rich
429 medium and standard laboratory conditions. Although our pull-down and bacterial-two hybrid data
430 indicate a probable interaction between RNase E and ArcB, a catabolic ornithine carbamoyltransferase
431 from the arginine deaminase pathway [78], no direct protein-protein binding could be observed in vitro,
432 nor were the two proteins colocalising in vivo. We propose that RNase E indirectly interacts with ArcB,
433 probably in a RNA-dependent manner. Indeed, the *arcDABC* polycistronic transcript is cleaved at
434 multiple sites by RNase E for its processing [79], suggesting that an regulatory interaction between
435 RNase E and ArcB polypeptide could occur during co-translational RNA cleavage [18].
436 Additionally, the RNase E-based RNA degradosome of *P. haloplanktis, P. syringae*, and *R. capsulatus*
437 do not seem to contain either a metabolic enzyme upon standard growing conditions [40-42]. This lack
438 of RNase E interaction with metabolic enzymes may reflect distinct physiological roles of the RNA
439 degradosome in different bacterial species, potentially linked to specific metabolic adaptations or
440 regulatory mechanisms that modulate RNA stability and processing depending on nutrient availability.
441 However, we cannot exclude that some protein partners were missed. Transient or condition-specific
442 accessory protein partners remain to be identified, and compositional biases such as the conserved
443 AEPV-rich part of the RNase E CTD are not yet understood, as no ligand or biological function has
444 been assigned to this region even in well-studied RNase E orthologs.

445 It is also important to mention that throughout this study, we chose to focus on core RNA degradosome
446 components that are identified based on their binding to RNase E CTD, but we cannot exclude that
447 some functional interactions occur with the NTD. For example, RhlB was found to interact with RNase
448 E NTD in *C. crescentus* [36], while in *Anabaena* the RNA helicase CrhB, RNase II and enolase were
449 shown to associate with RNase E via its NTD [38, 39]. Similarly, we found that the *P. aeruginosa*
450 RhlE2 RNA helicase, previously shown to associate with RNase E in an RNA-dependent manner [55],
451 interacts with the N-terminal domain of Pa RNase E. Although RhlE2 is not considered a core RNA
452 degradosome component based on our assumption of CTD-mediated interactions, this association
453 remains functionally significant [55, 56].
454 In the second part of our study, we evaluated the importance of RNA degradosome assembly at both
455 transcriptomic and phenotypic levels through an analysis of *P. aeruginosa* strains carrying RNase E
456 CTD truncations and mutations. Comparing the *rne588* and *rne529* strains allows us to discuss the
457 importance of RNA degradosome assembly and membrane attachment in *P. aeruginosa*. The two
458 mutants exhibited varying degrees of sensitivity to cold growth, with *rne529* being the most affected,
459 indicating that cold growth requires both RNase E membrane attachment and RNA degradosome
460 assembly. Loss of the CTD without delocalisation from the membrane (*rne588*) does not affect growth
461 in *P. aeruginosa* under standard laboratory condition (i.e., 37°C and rich medium), but impacts its
462 capacity to sustain growth in the cold. Transcripts levels were also generally affected in the mutants, as
463 well as global RNA degradation, as shown in the 5' read ends analysis. Decreased degradation of
464 cleaved transcripts could lead to an upregulation of their levels. Therefore, direct and indirect effects
465 remain to be distinguished and those changes remain to be correlated with proteins levels.
466 Surprisingly, we did not find any phenotypic changes associated to the loss of RhlB or PNPase binding,
467 questioning the importance of the RNA degradosome protein association for the complex functionality.
468 Competition assays could be useful in identifying any fitness defects in our mutants, as done in *E. coli*
469 for RNase E CTD truncations [19, 63], or different phenotypes or stresses could be tested.
470 On the other hand, our phenotypic analysis highlights the crucial role of CTD RNA binding for the
471 functionality of the RNA degradosome complex. Mutations in the SLiMs responsible for RNA binding
472 (AR1, AR4, and the REER-repeats) not only impair in vivo RNA degradosome foci assembly and/or
473 stability but also lead to decreased *P. aeruginosa* virulence and reduced growth at both 37°C and cold
474 temperatures. The effect of these mutations on foci formation mirrors the effect observed upon cell
475 exposure to rifampicin, which decreases RNA levels in the cell, and aligns with previous studies
476 showing that Ec and Cc RNase E orthologs also assemble foci in a CTD-dependent and RNA-dependent
477 manner [61-63]. Our data thus suggest that impairing foci formation has a major effect on the activity
478 of the RNA degradosome in *P. aeruginosa*.
479 Overall, our study identified core RNA degradosome components in *P. aeruginosa* and underscores the
480 role of this complex in bacterial adaptation to environmental changes and pathogenesis. By revealing
481 *P. aeruginosa*-specific interactions and their functional significance, our findings provide valuable

482 insights into the molecular mechanisms of adaptation in this pathogen and highlight the potential of the
483 RNA degradosome as a drug target.
484
485 **Methods**
486
487 **Bacterial strains and growing conditions**
488 A list of bacterial strains used can be found in Table S1. Unless otherwise specified, *P. aeruginosa* PAO1
489 was grown at 37°C in NYB (25 g of Difco nutrient broth, 5g of Difco yeast agar per liter) with shaking
490 at 180 rpm or on Nutrient Agar (NA) (40 g Oxoid blood agar base, 5 g Difco yeast agar per liter). When
491 required, antibiotics were added to these media at the following concentrations: 100 µg/ml ampicillin,
492 50 µg/mL kanamycin, 20 µg/mL tetracycline and 10 µg/ml gentamicin for *E. coli*; and 50 µg/mL or 100
493 µg/mL tetracycline and 50 µg/ml gentamicin for *P. aeruginosa*.
494
495 **Construction of plasmids used in this study**
496 Information about plasmid construction and primers used in this study can be found in supplementary
497 tables S2 and S3, respectively. Plasmids pUT18C and pKT25 were generally cloned by restriction
498 enzyme digestion using EcoRI-HF and BamHI-HF (NEB). When a gene to be inserted could be
499 internally cleaved by EcoRI and/or BamHI, the enzymes MfeI and/or BglII, respectively, were chosen
500 instead during primer design to allow ligation of the insert to the vector digested with EcoRI/BamHI
501 thanks to compatible cohesive ends. For cloning of *gdhB* into pKT25, NEB assembly® was used instead,
502 due to the presence of many restriction enzymes internal cleavage sites. Ligation reactions were carried
503 our using T4 DNA ligase (Roche or NEB) at 16°C overnight, or at room temperature for 2-3 hours,
504 following standard protocols. When cloning inserts into the suicide vectors pME3087 or pEXG2, the
505 NEBuilder HiFi DNA assembly Master Mix (NEB) was used according to the manufacturer's
506 recommendations. To constructs RNase E CTD mutants, the DNA was synthesized by GeneArt
507 (ThermoFisher Scientific) and cloned into appropriate vectors for protein purification or strain
508 construction as described in Table S4. To construct pME6032-based expression vectors, restriction
509 enzyme digestion was carried out using EcoRI and KpnI for both vector and inserts.
510 Ligation mixtures or the assembly reactions were transformed into chemically competent *E. coli* DH5α
511 cells by heat-shock, plating on appropriate selective LB agar medium. The resulting colonies were
512 screened by PCR for the presence of the insert in the plasmid of interest. After plasmid extraction
513 (Miniprep kit, Sigma-Aldrich/Merck), plasmids were verified by Sanger sequencing at Microsynth.
514
515 **Construction of *P. aeruginosa* mutant strains**
516 To construct chromosomal gene truncations or insert a Strep-tag or fluorescent protein into the
517 chromosome, in frame with a gene of interest, the suicide vectors pEXG2 [80] or pME3087 [81] were
518 used. Briefly, approximately 500 bp regions located immediately upstream or downstream of the region

519 to be edited, and, when applicable, the tag or fluorescent protein of interest, were amplified by PCR and
520 inserted together into the vector backbone using NEB assembly®. After sequencing verification of the
521 constructed plasmid quality, the plasmids were introduced into *P. aeruginosa* PAO1 strain by triparental
522 mating using the *E. coli* strain HB101 (pRK2013). After selection with the appropriate antibiotic
523 (tetracycline for pME3087 or gentamicin for pEXG2), merodiploids were resolved as described in [82]
524 for pME3087 or [80] for pEXG2, and strains with the desired insertion/deletion were identified by
525 colony PCR.
526
527 **RNase E sequence analysis**
528 Group-specific homologs of RNase E in *P. aeruginosa*, *P. fluorescens*, *P. protegens*, *P. putida* and *P.*
529 *stutzeri* were retrieved from NCBI databases using blastp [92] with *P. aeruginosa* PAO1 RNase E as a
530 query; only sequences with query coverage > 0.5 were conserved (total of 5000 proteins). The number
531 of RE[E/D]R motifs in each protein sequence was determined using the vcountPattern function from
532 the "biostrings" R package [93]. The similarity of the protein sequences within a taxonomic group was
533 determined using the conserv function (method="similarity") from the bio3D R package on a muscle
534 alignment of the protein sequences[94, 95].
535
536 **Electrophoretic motility shift assay**
537 The *malEF* transcript was synthesized with a T7 transcription kit (Invitrogen) on linear DNA template
538 (172 bp) obtained by PCR with primers p253-p254 (Table Sx). The electrophoretic mobility shift assay
539 (EMSA) was performed following the protocol of [86]. Briefly, the reaction mixtures (15 µl) contained
540 35 nM of RNA, 50mM Tris-HCl, 100mM NaCl, 5mM DTT, 1.0 units/µl RNasin (Promega), and
541 increasing concentrations of the His10Smt3-RNase E proteins (see Figure legends). The reactions were
542 incubated at 4 °C for 30 min before loading on 2% agarose gel and run at 150 V for 15 min. RNA bands
543 were visualized by gel staining with SybrGold (Invitrogen).
544
545 **Epifluorescence microscopy imaging**
546 Phase contrast and fluorescence microscopy were performed on a Zeiss Axio Imager 2 equipped with
547 an objective alpha Plan-Apochromat 100x/1,46 Oil Ph3 M27 and a ZEISS Axiocam 305 mono CCD
548 camera. Bacteria were grown until OD_{600nm}= 0.2-0.6 (approx. 2.5 hours) in 3 ml of NYB and were then
549 placed on an agarose pad containing 1% agarose dissolved in 0.5X PBS. Images were processed with
550 Fiji (NIH, USA) [84].
551
552 **Image analysis**
553 All image treatments and analysis were performed using Fiji (NIH, USA)[84]. Representative images
554 shown had contrast adjusted for display by opening the images in Fiji and using the Reset function in
555 the Adjust Brightness/Contrast menu, after average background intensity subtraction using the Math ->

556 Subtract function. These average background intensity values were obtained by measuring a square area
557 devoid of any cells. For quantification of signal intensity, a line was drawn alongside the long axis of
558 bacterial cells and signal was measured using Plot Profile. Results of this function were saved as .csv
559 files. For each strain, at least 50 bacterial cells were measured from the raw images, using at least two
560 different images for quantification. Average background values were subsequently subtracted from each
561 results file using a .csv file containing the Plot Profile measurements of a linear area devoid of cells for
562 each image used. Fluorescence intensity was measured along the longitudinal axis of the cells in 50-
563 100 cells using Fiji. Boxplots of fluorescence intensity and signal variance were plotted using R [85].
564 The signal variance was obtained by calculating the variance of the $\log_2$ fold-change between each
565 measured value and the average of all values for a given measured cell. This was done to normalize the
566 data and obtain comparable variances without introducing a bias due to differences in overall signal
567 intensity.
568
569 **Pull-down identification of RNase E partners**
570 Fresh cultures of PAO1 WT, PAO1 RNase E_{1-529}-Strep, or PAO1 RNase E_{1-1057}-Strep were inoculated to
571 OD=0.05 from overnight cultures in 500 mL Erlenmeyer flasks. Cultures were grown until approx.
572 OD_{600nm}=0.8-0.9. 50 mL of each culture was harvested by centrifugation at 4500 *x g* for 10 minutes.
573 Pellets were stored at -80°C until needed.
574 Each thawed pellet was then resuspended in 3,25 mL of lysis buffer (for 10 mL of buffer, prepared just
575 before use: 20 mM Tris (pH 10), 250 mM NaCl, 10% v/v glycerol, 1 EDTA-free protease inhibitor
576 tablet, 50 µg/mL lysozyme). Samples were incubated the samples on ice for about 30 minutes,
577 transferred into 15-mL Falcon tubes and sonicated using a thin probe for 6x30s, with 15 seconds break
578 in between. A pulse of 70% and a power output of 50% were used. After sonication, 32.5 µL of Triton
579 X100 10% were added to each sample (~0.1% final) before incubation on a rotary wheel at 4°C for 8
580 minutes. The samples were transferred into 2 mL Eppendorf tubes and centrifuged for 1 hour at 10500
581 *x g* at 4°C. MagStrep® Strep-Tactin®XT beads (IBA, cat# 2-5090) were washed in wash buffer (20 mM
582 Tris (pH 10), 250 mM NaCl, 10% v/v glycerol) according to the manufacturer's instructions. One mix
583 of beads was prepared for all the samples with a volume of beads suspension of 45 µL per sample. Final
584 resuspension was done in 200 µL wash buffer per sample, plus an additional 10 µL. After centrifugation
585 of the samples, the supernatant of each sample was regrouped into a 5 mL Eppendorf tube, and 200 µL
586 of washed beads suspension were added per sample. Incubation on a rotary wheel was done for 2h15 at
587 4°C. The 5 mL tubes were then placed against a magnetic rack and all the supernatant was carefully
588 removed. A first wash volume of 500 µL was added gently and agitated by horizontal rotations of the
589 tubes. Tubes were placed back against the magnetic rack and the wash volume was removed. A second
590 wash step was performed identically with a volume of 225 µL instead of 500 µL. A third wash step of
591 225 µL was also performed, and the resuspended beads were transferred into a clean 1.5 mL Eppendorf
592 tube by gentle pipetting with a 1000 µL tip, before removing the wash volume. The beads were covered

593 with 10 µL of sterile PBS and stored at 4°C before LC-MS/MS analysis at the Proteomics Core Facility
594 (University of Geneva). For plots in Fig. 3A-B, the log2 fold-change (log2FC) was calculated using the
595 following formula: log2(average peptide count of protein *x* identified in the RNase $E^{1\text{-}xxx}$-Strep / average
596 peptide count of protein *x* identified in the untagged sample).When an average count of 0 peptide was
597 identified in the untagged sample, the log2FC value was instead calculated using the following formula:
598 log2FC(average peptide count of protein *x* identified in the RNase $E^{1\text{-}xxx}$-Strep/1).
599

600 **Bacterial adenylate cyclase two-hybrid assay**

601 Cloned plasmids were introduced into chemically competent BTH101 cells by heat shock, and the cells
602 were plated in LB agar supplemented with ampicillin and kanamycin. Isolated colonies were then
603 streaked as a line of about 1-2 cm on freshly prepared Mac Conkey agar medium supplemented with
604 ampicillin, kanamycin, 0.5 mM isopropyl β-d-thiogalactoside (IPTG), and maltose 1%. The
605 MacConkey Petri dishes were then incubated at 30°C for 24h followed by an incubation at room
606 temperature (~23°C) for 24h. The bacteria were imaged by scanning the plates, after which
607 quantification of β-galactosidase activity was done using ONPG as described in [83].
608

609 **Protein purification**

610 His_{10}Smt3-tagged PNPase and His_{10}Smt3-tagged RhlB proteins were purified from soluble bacterial
611 lysates by nickel-agarose affinity chromatography as described previously in the supplementary
612 information of Hausmann *et al.* 2021 [55]. The imidazole elution profiles were monitored by SDS-
613 PAGE. The recombinant His_{10}Smt3-tagged proteins were recovered predominantly in the 250 mM
614 imidazole fraction, shown in Figure 4 (input lane I). Protein concentration was determined using the
615 Bio-Rad dye reagent, with BSA as the standard, and calculated by interpolation against the BSA
616 standard curve. The His_{10}-Smt3 tag remained uncleaved in the protein-protein interaction assays. Note
617 that the His_{10}Smt3-tagged proteins do not bind to RNase E fusion proteins (data not shown).
618 RNase $E_{1\text{-}529}$, RNase $E_{572\text{-}1057}$, RNase $E_{572\text{-}1057_NDPRmut}$, and RNase $E_{572\text{-}1057_AR1mut}$ proteins, each carrying
619 a His_{10}Smt3 tag at the N-terminus and a Twin-Strep-tag®-Flag at the C-terminus, were purified as
620 described above. The 250 mM imidazole elution fractions were used directly in the Protein-Protein
621 interaction assays. For the EMSA experiment, the RNase E proteins were further purified as follows:
622 the 250 mM imidazole fraction were applied to a 1 ml of Strep-Tactin Sepharose (Iba) column that had
623 been equilibrated with buffer C (50 mM Tris pH8, 200 mM NaCl, 10 % glycerol). The column was
624 washed with 5 ml of buffer C and then eluted stepwise with 1 ml aliquots of buffer C containing, 2.5
625 mM D-Desthiobiotin respectively. The elution profiles were monitored by SDS-PAGE (not shown).
626

627 **Protein-protein interaction assays**

628 Purified RNase $E_{1\text{-}529}$-Flag, RNase $E_{572\text{-}1057}$-Flag, RNase $E_{572\text{-}1057_NDPRmut}$- Flag, or RNase $E_{572\text{-}1057_AR1mut}$-

629 Flag fusion proteins (20-25 µg each) were incubated for 1 hour at 4 °C on a rotating device with 25 µl
630 of Anti-Flag M2 magnetic beads (Sigma M8823) in 100 µl of binding buffer H (50 mM Tris-HCl, pH
631 8.0, 150 mM NaCl, 0.01% Triton X-100). The beads were then collected using a magnetic separator
632 and washed three times with 0.25 ml of binding buffer H to remove any unbound protein.
633 For affinity chromatography, the anti-Flag magnetic beads (Sigma-Aldrich) with bound RNase E-Flag
634 fusion proteins, or beads alone, were incubated with either 5 µg of PNPase (Figure 4A) or 5 µg of RhlB
635 (Figure 4B) in 100 µl of binding buffer H for 1 hour at 4 °C on a rotating device. After incubation, the
636 beads were collected using the magnet, and the supernatant (free fraction F) was withdrawn. The anti-
637 Flag beads were then resuspended in 100 µl of binding buffer H and subjected to three rounds of
638 washing. Following the final wash, the protein bound to the beads was eluted with 100 µl of 2X LDS
639 sample buffer (Invitrogen). Aliquots (15 µl) of the input protein sample (PNPase or RhlB), the first
640 supernatant fraction (free fraction F), and the bead-bound fraction were mixed with 5 µl of 4X LDS
641 sample buffer (Invitrogen), heated at 80 °C for 5 minutes, and analysed by SDS-PAGE. Polypeptides
642 were visualized using Coomassie Blue staining.
643
644 **Growth assays on solid or liquid media**
645 To assess the growth of the mutant strains in liquid medium, 200 µL of NYB broth was inoculated to
646 OD_{600nm}=0.05 in a 96-well plate, using an overnight culture washed twice with fresh medium. The wells
647 on the edge of the plate were not used. The plate was incubated at 37°C using a Biotek Synergy H1
648 Hybrid Plate reader. OD_{600nm} values were measured every 30 minutes. Before each OD_{600nm}
649 measurement, orbital shaking with 282 cpm (3 mm) was performed for 1 minute. Data was retrieved
650 the following day and plotted after substraction of blank OD_{600nm} values using GraphPad Prism.
651 When growing strains carrying the pME6032 vector for complementation assays, NYB medium was
652 supplemented with 50 µg/mL of Tetracycline and 70 µM of IPTG for induction. Cells were resuspended
653 in supplemented NYB after washing and before inoculating the 96-well plate.
654 To assess the growth of the mutant strains on solid medium, square Petri dishes (12x12cm) were filled
655 with 50 mL of warm NA. When testing growth at low vs high pH, either 75 µL of 37% fuming HCl or
656 400 µL of 5N NaOH was added per 50 mL of NA agar to achieve the desired conditions. A fresh culture
657 (OD_{600nm}= 0.4-0.8) of each strain was adjusted to OD_{600nm}=1 by centrifugation and serially diluted in a
658 96-well plate using a multipipette. 5 µL of each dilution series was then spotted using a multipipette
659 onto pre-dried NA plates (1 hour under a sterile flowhood). After the spots had dried, plates were
660 incubated upside down at 37°C or 16°C.
661
662 **Galleria killing assays**
663 *Galleria mellonella* larvae were used to assess in vivo virulence and/or survival of several RNase E
664 mutant strains. Fresh cultures were adjusted to a suspension of OD_{600nm}= 1 and serially diluted to 10^{-6}
665 in Gibco Dulbecco's Phosphate Buffered Saline (dPBS) (Thermo Fisher Scientific). 10 µL of the 10^{-6}

666 dilution were spotted onto NYB agar to verify that the dilutions were similar for the different strains.
667 10 µL spots were then put onto a clean parafilm and injected using Omnican 50 sterile insulin syringe
668 (Braun) into the second to last leg of the larvae, facing towards the head. As a control, sterile dPBS was
669 injected similarly into larvae to assess background levels of death. For every 10 larvae injected, the time
670 of injection was recorded, and they were placed inside a dark incubator at 37°C. The next day, deaths
671 were recorded every hour. A larva was considered dead when it completely stopped responding to
672 stimuli (touched on the legs or the head with a pipette tip). Survival curves were plotted and analysed
673 with GraphPad Prism (GraphPad Software, Prism10.2).
674
675 **RNA-seq sample collection**
676 PAO1 WT, PAO1 RNase E_{1-588}, (*rne588*) and PAO1 RNase E_{1-529} (*rne529*) strains were grown in 50 mL
677 Erlenmeyer flasks (10 mL NYB broth) until OD_{600nm}= 1.0-1.2. 500 µL of culture were immediately
678 added into four separate 1.5 mL tubes, each containing 1 mL of RNAlater (Sigma-Aldrich, cat). After
679 harvesting of all three strains, the tubes were centrifuged for 30 minutes at 9600 x *g*. Supernatant was
680 discarded and pellets were stored at -80°C until RNA extraction. The RNA extraction was performed
681 using two tubes of pellets for each strain, with the Monarch Total RNA Miniprep kit. For lysis of the
682 bacterial cells, the two pellets were resuspended in 250 µL of 1X Tris-EDTA (TE) buffer supplemented
683 with 1 mg/mL of lysozyme and regrouped into one tube for each strain, incubated for 5 minutes at RT,
684 and RNA was subsequently extracted following the manufacturer's instructions. After RNA
685 purification, an additional DNA removal treatment was done using TURBO DNase (Thermo Fisher)
686 according to the manufacturer's instructions. RNA was purified again using the RNA purification
687 columns (dark blue) from the Monarch Total RNA Miniprep kit, and following the priming, washing
688 and elution steps described by the manufacturer. The absence of residual gDNA contamination was
689 verified by performing a PCR for 35 cycles using primer pairs targeting *rpoD* [55]. Biological triplicate
690 samples for each strain were prepared. Quality check, ribosomal RNA depletion and RNA sequencing
691 were conducted by Novogene.
692
693 **RNA sequencing analysis**
694 Reads were mapped using Bowtie2 [87] to *Pseudomonas aeruginosa* PAO1 genome assembly
695 ASM676v1 and counts were aggregated using summarize Overlaps in the package GenomicAlignments
696 [88] in R using the ASM676v1 gtf version 2.2 (NCBI accession: GCF_000006765.1). Differential
697 expression was performed using DESeq2 [89] and transcripts were considered differentially expressed
698 between two conditions if the absolute value of log2FC between conditions was greater than 1 (i.e. 2-
699 fold up or down) with a p-value less than 0.05. To find functional enrichment among differentially
700 expressed genes groups, the Kyoto Encyclopedia of Genes and Genomes (KEGG) was used for gene
701 set definitions, downloaded using the package KEGGREST [90] in R. Enrichment was calculated using
702 a hypergeometric test. All correlations presented are Pearson's product moment correlation coefficient.

Pairwise correlations of log2 Reads Per Kilobase per Million mapped reads (RPKMs) and hierarchical unsupervised clustering analysis of fold changes relative to WT demonstrate the similarity in the profile of the biological replicates for each strain. Analysis of 5' read ends per loci was performed as described by de Araújo et al. [91] except that each dataset read number was down-sampled to 8 million.

Acknowledgments

We thank Sylvain Guex-Crosier for his assistance with RNA extraction and Nathanaël Guggenheim for protein purification and assistance with cloning experiments. We also acknowledge the Proteomics Core Facility and the Bioinformatics Support Platform from the University of Geneva for assistance with the realisation of LC-MS-MS and bioinformatics analyses, respectively.

713 **References**

714

715 1. Hui MP, Foley PL, Belasco JG. Messenger RNA Degradation in Bacterial Cells. Annual Review
716 of Genetics. 2014;48(1):537-59. doi: 10.1146/annurev-genet-120213-092340. PubMed PMID:
717 25292357.

718 2. Celesnik H, Deana A, Belasco JG. Initiation of RNA decay in *Escherichia coli* by 5'
719 pyrophosphate removal. Mol Cell. 2007;27(1):79-90. doi: 10.1016/j.molcel.2007.05.038. PubMed
720 PMID: 17612492; PubMed Central PMCID: PMCPMC2196405.

721 3. Deana A, Celesnik H, Belasco JG. The bacterial enzyme RppH triggers messenger RNA
722 degradation by 5' pyrophosphate removal. Nature. 2008;451(7176):355-8. doi: 10.1038/nature06475.
723 PubMed PMID: 18202662.

724 4. Luciano DJ, Vasilyev N, Richards J, Serganov A, Belasco JG. Importance of a diphosphorylated
725 intermediate for RppH-dependent RNA degradation. RNA Biol. 2018;15(6):703-6. Epub 20180529.
726 doi: 10.1080/15476286.2018.1460995. PubMed PMID: 29619898; PubMed Central PMCID:
727 PMCPMC6152431.

728 5. Tejada-Arranz A, de Crecy-Lagard V, de Reuse H. Bacterial RNA Degradosomes: Molecular
729 Machines under Tight Control. Trends Biochem Sci. 2020;45(1):42-57. Epub 20191101. doi:
730 10.1016/j.tibs.2019.10.002. PubMed PMID: 31679841; PubMed Central PMCID: PMCPMC6958999.

731 6. Dressaire C, Picard F, Redon E, Loubière P, Queinnec I, Girbal L, Cocaign-Bousquet M. Role
732 of mRNA stability during bacterial adaptation. PLoS One. 2013;8(3):e59059. PubMed PMID:
733 23516597.

734 7. Broglia L, Le Rhun A, Charpentier E. Methodologies for bacterial ribonuclease characterization
735 using RNA-seq. FEMS Microbiol Rev. 2023;47(5). PubMed PMID: 37656885.

736 8. Ono M, Kuwano M. A conditional lethal mutation in an *Escherichia coli* strain with a longer
737 chemical lifetime of messenger RNA. J Mol Biol. 1979;129(3):343-57. Epub 1979/04/15. doi:
738 10.1016/0022-2836(79)90500-x. PubMed PMID: 110942.

739 9. Apirion D. Isolation, genetic mapping and some characterization of a mutation in *Escherichia*
740 *coli* that affects the processing of ribonuleic acid. Genetics. 1978;90(4):659-71. PubMed PMID:
741 369943.

742 10. Jain C, Deana A, Belasco JG. Consequences of RNase E scarcity in *Escherichia coli*. Molecular
743 Microbiology. 2002;43(4):1053-64. doi: https://doi.org/10.1046/j.1365-2958.2002.02808.x.

744 11. Caruthers JM, Feng Y, McKay DB, Cohen SN. Retention of core catalytic functions by a
745 conserved minimal ribonuclease E peptide that lacks the domain required for tetramer formation. J Biol
746 Chem. 2006;281(37):27046-51. Epub 20060719. doi: 10.1074/jbc.M602467200. PubMed PMID:
747 16854990.

12. Callaghan AJ, Aurikko JP, Ilag LL, Günter Grossmann J, Chandran V, Kühnel K, et al. Studies of the RNA degradosome-organizing domain of the *Escherichia coli* ribonuclease RNase E. J Mol Biol. 2004;340(5):965-79. doi: 10.1016/j.jmb.2004.05.046. PubMed PMID: 15236960.

13. Carpousis AJ, Van Houwe G, Ehretsmann C, Krisch HM. Copurification of E. coli RNAase E and PNPase: evidence for a specific association between two enzymes important in RNA processing and degradation. Cell. 1994;76(5):889-900. doi: 10.1016/0092-8674(94)90363-8. PubMed PMID: 7510217.

14. Py B, Higgins CF, Krisch HM, Carpousis AJ. A DEAD-box RNA helicase in the *Escherichia coli* RNA degradosome. Nature. 1996;381(6578):169-72. doi: 10.1038/381169a0. PubMed PMID: 8610017.

15. Chandran V, Luisi BF. Recognition of enolase in the Escherichia coli RNA degradosome. J Mol Biol. 2006;358(1):8-15. Epub 20060221. doi: 10.1016/j.jmb.2006.02.012. PubMed PMID: 16516921.

16. Worrall JAR, Górna M, Crump NT, Phillips LG, Tuck AC, Price AJ, et al. Reconstitution and Analysis of the Multienzyme Escherichia coli RNA Degradosome. Journal of Molecular Biology. 2008;382(4):870-83. doi: https://doi.org/10.1016/j.jmb.2008.07.059.

17. Bandyra KJ, Bouvier M, Carpousis AJ, Luisi BF. The social fabric of the RNA degradosome. Biochim Biophys Acta. 2013;1829(6-7):514-22. Epub 20130228. doi: 10.1016/j.bbagrm.2013.02.011. PubMed PMID: 23459248; PubMed Central PMCID: PMCPMC3991390.

18. Tsai YC, Du D, Domínguez-Malfavón L, Dimastrogiovanni D, Cross J, Callaghan AJ, et al. Recognition of the 70S ribosome and polysome by the RNA degradosome in *Escherichia coli*. Nucleic Acids Res. 2012;40(20):10417-31. Epub 20120825. doi: 10.1093/nar/gks739. PubMed PMID: 22923520; PubMed Central PMCID: PMCPMC3488216.

19. Leroy A, Vanzo NF, Sousa S, Dreyfus M, Carpousis AJ. Function in *Escherichia coli* of the non-catalytic part of RNase E: role in the degradation of ribosome-free mRNA. Mol Microbiol. 2002;45(5):1231-43. doi: 10.1046/j.1365-2958.2002.03104.x. PubMed PMID: 12207692.

20. Dendooven T, Paris G, Shkumatov AV, Islam MS, Burt A, Kubańska MA, et al. Multi-scale ensemble properties of the *Escherichia coli* RNA degradosome. Mol Microbiol. 2022;117(1):102-20. Epub 20210925. doi: 10.1111/mmi.14800. PubMed PMID: 34415624; PubMed Central PMCID: PMCPMC7613265.

21. Sinha D, De Lay NR. Target recognition by RNase E RNA-binding domain AR2 drives sRNA decay in the absence of PNPase. Proc Natl Acad Sci U S A. 2022;119(48):e2208022119. Epub 20221121. doi: 10.1073/pnas.2208022119. PubMed PMID: 36409892; PubMed Central PMCID: PMCPMC9860253.

22. Lee K, Zhan X, Gao J, Qiu J, Feng Y, Meganathan R, et al. RraA. a protein inhibitor of RNase E activity that globally modulates RNA abundance in *E. coli*. Cell. 2003;114(5):623-34. PubMed PMID: 13678585.

23. Górna MW, Pietras Z, Tsai YC, Callaghan AJ, Hernández H, Robinson CV, Luisi BF. The regulatory protein RraA modulates RNA-binding and helicase activities of the E. coli RNA degradosome. Rna. 2010;16(3):553-62. Epub 20100127. doi: 10.1261/rna.1858010. PubMed PMID: 20106955; PubMed Central PMCID: PMCPMC2822920.

24. Gao J, Lee K, Zhao M, Qiu J, Zhan X, Saxena A, et al. Differential modulation of E. coli mRNA abundance by inhibitory proteins that alter the composition of the degradosome. Mol Microbiol. 2006;61(2):394-406. Epub 20060612. doi: 10.1111/j.1365-2958.2006.05246.x. PubMed PMID: 16771842.

25. Prud'homme-Généreux A, Beran RK, Iost I, Ramey CS, Mackie GA, Simons RW. Physical and functional interactions among RNase E, polynucleotide phosphorylase and the cold-shock protein, CsdA: evidence for a 'cold shock degradosome'. Molecular Microbiology. 2004;54(5):1409-21. doi: https://doi.org/10.1111/j.1365-2958.2004.04360.x.

26. Blum E, Py B, Carpousis AJ, Higgins CF. Polyphosphate kinase is a component of the Escherichia coli RNA degradosome. Molecular Microbiology. 1997;26(2):387-98. doi: https://doi.org/10.1046/j.1365-2958.1997.5901947.x.

27. Kannaiah S, Goldberger O, Alam N, Barnabas G, Pozniak Y, Nussbaum-Shochat A, et al. MinD-RNase E interplay controls localization of polar mRNAs in E. coli. Embo j. 2024;43(4):637-62. Epub 20240119. doi: 10.1038/s44318-023-00026-9. PubMed PMID: 38243117; PubMed Central PMCID: PMCPMC10897333.

28. Taghbalout A, Rothfield L. RNaseE and the other constituents of the RNA degradosome are components of the bacterial cytoskeleton. Proceedings of the National Academy of Sciences. 2007;104(5):1667-72. doi: 10.1073/pnas.0610491104.

29. Ikeda Y, Yagi M, Morita T, Aiba H. Hfq binding at RhlB-recognition region of RNase E is crucial for the rapid degradation of target mRNAs mediated by sRNAs in Escherichia coli. Mol Microbiol. 2011;79(2):419-32. Epub 20101118. doi: 10.1111/j.1365-2958.2010.07454.x. PubMed PMID: 21219461.

30. Aït-Bara S, Carpousis AJ, Quentin Y. RNase E in the γ-Proteobacteria: conservation of intrinsically disordered noncatalytic region and molecular evolution of microdomains. Mol Genet Genomics. 2015;290(3):847-62. Epub 20141129. doi: 10.1007/s00438-014-0959-5. PubMed PMID: 25432321; PubMed Central PMCID: PMCPMC4435900.

31. Goldblum K, Apririon D. Inactivation of the ribonucleic acid-processing enzyme ribonuclease E blocks cell division. J Bacteriol. 1981;146(1):128-32. doi: 10.1128/jb.146.1.128-132.1981. PubMed PMID: 6163761; PubMed Central PMCID: PMCPMC217061.

32. Bernstein JA, Lin PH, Cohen SN, Lin-Chao S. Global analysis of *Escherichia coli* RNA degradosome function using DNA microarrays. Proc Natl Acad Sci U S A. 2004;101(9):2758-63. Epub 20040223. doi: 10.1073/pnas.0308747101. PubMed PMID: 14981237; PubMed Central PMCID: PMCPMC365694.

821 33. Kido M, Yamanaka K, Mitani T, Niki H, Ogura T, Hiraga S. RNase E polypeptides lacking a
822 carboxyl-terminal half suppress a mukB mutation in *Escherichia coli*. J Bacteriol. 1996;178(13):3917-
823 25. doi: 10.1128/jb.178.13.3917-3925.1996. PubMed PMID: 8682798; PubMed Central PMCID:
824 PMCPMC232654.
825 34. Lopez PJ, Marchand I, Joyce SA, Dreyfus M. The C-terminal half of RNase E, which organizes
826 the *Escherichia coli* degradosome, participates in mRNA degradation but not rRNA processing in vivo.
827 Mol Microbiol. 1999;33(1):188-99. doi: 10.1046/j.1365-2958.1999.01465.x. PubMed PMID:
828 10411735.
829 35. Hardwick SW, Chan VS, Broadhurst RW, Luisi BF. An RNA degradosome assembly in
830 *Caulobacter crescentus*. Nucleic Acids Res. 2011;39(4):1449-59. Epub 20101015. doi:
831 10.1093/nar/gkq928. PubMed PMID: 20952404; PubMed Central PMCID: PMCPMC3045602.
832 36. Voss JE, Luisi BF, Hardwick SW. Molecular recognition of RhlB and RNase D in the
833 *Caulobacter crescentus* RNA degradosome. Nucleic Acids Res. 2014;42(21):13294-305. Epub
834 20141111. doi: 10.1093/nar/gku1134. PubMed PMID: 25389270; PubMed Central PMCID:
835 PMCPMC4245959.
836 37. Zhang JY, Deng XM, Li FP, Wang L, Huang QY, Zhang CC, Chen WL. RNase E forms a
837 complex with polynucleotide phosphorylase in cyanobacteria via a cyanobacterial-specific nonapeptide
838 in the noncatalytic region. RNA. 2014;20(4):568-79. Epub 20140221. doi: 10.1261/rna.043513.113.
839 PubMed PMID: 24563514; PubMed Central PMCID: PMCPMC3964918.
840 38. Yan HD, Qin XX, Wang L, Chen WL. Both Enolase and the DEAD-Box RNA Helicase CrhB
841 Can Form Complexes with RNase E in *Anabaena* sp. Strain PCC 7120. Applied and environmental
842 microbiology. 2020;86(13). doi: 10.1128/AEM.00425-20. PubMed PMID: WOS:000546650600011.
843 39. Zhou C, Zhang JY, Hu XY, Li CC, Wang L, Huang QY, Chen WL. RNase II binds to RNase E
844 and modulates its endoribonucleolytic activity in the cyanobacterium *Anabaena* PCC 7120. Nuceic
845 Acid Res. 2020;48(7):3922-34. doi: 10.1093/nar/gkaa092. PubMed PMID: WOS:000525957700040.
846 40. Purusharth RI, Klein F, Sulthana S, Jäger S, Jagannadham MV, Evguenieva-Hackenberg E, et
847 al. Exoribonuclease R Interacts with Endoribonuclease E and an RNA Helicase in the Psychrotrophic
848 Bacterium Pseudomonas syringae Lz4W*. Journal of Biological Chemistry. 2005;280(15):14572-8.
849 doi: https://doi.org/10.1074/jbc.M413507200.
850 41. Jäger S, Fuhrmann O, Heck C, Hebermehl M, Schiltz E, Rauhut R, Klug G. An mRNA
851 degrading complex in *Rhodobacter capsulatus*. Nucleic Acids Res. 2001;29(22):4581-8. doi:
852 10.1093/nar/29.22.4581. PubMed PMID: 11713307; PubMed Central PMCID: PMCPMC92556.
853 42. Aït-Bara S, Carpousis Agamemnon J. Characterization of the RNA Degradosome of
854 *Pseudoalteromonas haloplanktis*: Conservation of the RNase E-RhlB Interaction in the
855 Gammaproteobacteria. Journal of Bacteriology. 2010;192(20):5413-23. doi: 10.1128/jb.00592-10.

856 43. Hardwick SW, Gubbey T, Hug I, Jenal U, Luisi BF. Crystal structure of *Caulobacter crescentus*
857 polynucleotide phosphorylase reveals a mechanism of RNA substrate channelling and RNA
858 degradosome assembly. Open Biology. 2012;2(4):120028. doi: 10.1098/rsob.120028.
859 44. Nurmohamed S, Vaidialingam B, Callaghan AJ, Luisi BF. Crystal Structure of Escherichia coli
860 Polynucleotide Phosphorylase Core Bound to RNase E, RNA and Manganese: Implications for
861 Catalytic Mechanism and RNA Degradosome Assembly. Journal of Molecular Biology.
862 2009;389(1):17-33. doi: https://doi.org/10.1016/j.jmb.2009.03.051.
863 45. Green SK, Schroth MN, Cho JJ, Kominos SK, Vitanza-jack VB. Agricultural plants and soil as
864 a reservoir for *Pseudomonas aeruginosa*. Applied microbiology. 1974;28(6):987-91. Epub 1974/12/01.
865 PubMed PMID: 4217591; PubMed Central PMCID: PMCPMC186868.
866 46. Hardalo C, Edberg SC. *Pseudomonas aeruginosa*: assessment of risk from drinking water.
867 Critical reviews in microbiology. 1997;23(1):47-75. Epub 1997/01/01. doi:
868 10.3109/10408419709115130. PubMed PMID: 9097014.
869 47. Pendleton JN, Gorman SP, Gilmore BF. Clinical relevance of the ESKAPE pathogens. Expert
870 review of anti-infective therapy. 2013;11(3):297-308. Epub 2013/03/06. doi: 10.1586/eri.13.12.
871 PubMed PMID: 23458769.
872 48. https://www.who.int/news/item/27-02-2017-who-publishes-list-of-bacteria-for-which-new-
873 antibiotics-are-urgently-needed.
874 49. Garcia-Clemente M, de la Rosa D, Máiz L, Girón R, Blanco M, Olveira C, et al. Impact of
875 Pseudomonas aeruginosa Infection on Patients with Chronic Inflammatory Airway Diseases. Journal of
876 clinical medicine. 2020;9(12). Epub 2020/12/02. doi: 10.3390/jcm9123800. PubMed PMID: 33255354.
877 50. Urwin L, Okurowska K, Crowther G, Roy S, Garg P, Karunakaran E, et al. Corneal Infection
878 Models: Tools to Investigate the Role of Biofilms in Bacterial Keratitis. Cells. 2020;9(11). Epub
879 2020/11/14. doi: 10.3390/cells9112450. PubMed PMID: 33182687; PubMed Central PMCID:
880 PMCPMC7696224.
881 51. Costerton JW, Stewart PS, Greenberg EP. Bacterial biofilms: a common cause of persistent
882 infections. Science (New York, NY). 1999;284(5418):1318-22. Epub 1999/05/21. doi:
883 10.1126/science.284.5418.1318. PubMed PMID: 10334980.
884 52. Lu Q, Eggimann P, Luyt CE, Wolff M, Tamm M, François B, et al. Pseudomonas aeruginosa
885 serotypes in nosocomial pneumonia: prevalence and clinical outcomes. Critical care (London, England).
886 2014;18(1):R17. Epub 2014/01/17. doi: 10.1186/cc13697. PubMed PMID: 24428878; PubMed Central
887 PMCID: PMCPMC4057348.
888 53. Hancock RE. Resistance mechanisms in *Pseudomonas aeruginosa* and other nonfermentative
889 gram-negative bacteria. Clin Infect Dis. 1998;27 Suppl 1:S93-9. Epub 1998/08/26. PubMed PMID:
890 9710677.
891 54. Van den Bossche A, Hardwick SW, Ceyssens PJ, Hendrix H, Voet M, Dendooven T, et al.
892 Structural elucidation of a novel mechanism for the bacteriophage-based inhibition of the RNA

893 degradosome. Elife. 2016;5. Epub 20160722. doi: 10.7554/eLife.16413. PubMed PMID: 27447594;
894 PubMed Central PMCID: PMCPMC4980113.
895 55. Hausmann S, Gonzalez D, Geiser J, Valentini M. The DEAD-box RNA helicase RhlE2 is a
896 global regulator of *Pseudomonas aeruginosa* lifestyle and pathogenesis. Nucleic Acids Res.
897 2021;49(12):6925-40. doi: 10.1093/nar/gkab503. PubMed PMID: 34151378; PubMed Central PMCID:
898 PMCPMC8266600.
899 56. Hausmann S, Geiser J, Allen GE, Geslain SAM, Valentini M. Intrinsically disordered regions
900 regulate RhlE RNA helicase functions in bacteria. Nucleic Acids Res. 2024. Epub 20240614. doi:
901 10.1093/nar/gkae511. PubMed PMID: 38874491.
902 57. Sonnleitner E, Romeo A, Bläsi U. Small regulatory RNAs in *Pseudomonas aeruginosa*. RNA
903 Biol. 2012;9(4):364-71. Epub 2012/02/18. doi: 10.4161/rna.19231. PubMed PMID: 22336763.
904 58. Valentini M, Gonzalez D, Mavridou DA, Filloux A. Lifestyle transitions and adaptive
905 pathogenesis of *Pseudomonas aeruginosa*. Current opinion in microbiology. 2018;41:15-20. Epub
906 2017/11/23. doi: 10.1016/j.mib.2017.11.006. PubMed PMID: 29166621.
907 59. Ait-Bara S, Carpousis AJ, Quentin Y. RNase E in the gamma-Proteobacteria: conservation of
908 intrinsically disordered noncatalytic region and molecular evolution of microdomains. Mol Genet
909 Genomics. 2015;290(3):847-62. Epub 20141129. doi: 10.1007/s00438-014-0959-5. PubMed PMID:
910 25432321; PubMed Central PMCID: PMCPMC4435900.
911 60. Nishio S-y, Itoh T. Arginine-rich RNA binding domain and protein scaffold domain of RNase
912 E are important for degradation of RNAI but not for that of the Rep mRNA of the ColE2 plasmid.
913 Plasmid. 2009;62(2):83-7. doi: https://doi.org/10.1016/j.plasmid.2009.04.002.
914 61. Hamouche L, Poljak L, Carpousis AJ. Polyribosome-Dependent Clustering of Membrane-
915 Anchored RNA Degradosomes To Form Sites of mRNA Degradation in *Escherichia coli*. mBio.
916 2021;12(5):e0193221. Epub 20210907. doi: 10.1128/mBio.01932-21. PubMed PMID: 34488454;
917 PubMed Central PMCID: PMCPMC8546579.
918 62. Al-Husini N, Tomares DT, Bitar O, Childers WS, Schrader JM. α-Proteobacterial RNA
919 Degradosomes Assemble Liquid-Liquid Phase-Separated RNP Bodies. Mol Cell. 2018;71(6):1027-
920 39.e14. Epub 20180906. doi: 10.1016/j.molcel.2018.08.003. PubMed PMID: 30197298; PubMed
921 Central PMCID: PMCPMC6151146.
922 63. Khemici V, Poljak L, Luisi BF, Carpousis AJ. The RNase E of *Escherichia coli* is a membrane-
923 binding protein. Mol Microbiol. 2008;70(4):799-813. Epub 20081002. doi: 10.1111/j.1365-
924 2958.2008.06454.x. PubMed PMID: 18976283; PubMed Central PMCID: PMCPMC7610891.
925 64. Schuck A, Diwa A, Belasco JG. RNase E autoregulates its synthesis in Escherichia coli by
926 binding directly to a stem-loop in the rne 5' untranslated region. Mol Microbiol. 2009;72(2):470-8. Epub
927 20090306. doi: 10.1111/j.1365-2958.2009.06662.x. PubMed PMID: 19320830; PubMed Central
928 PMCID: PMCPMC2857391.

929 65. Liu S-J, Lin G-M, Yuan Y-Q, Chen W, Zhang J-Y, Zhang C-C. A conserved protein inhibitor
930 brings under check the activity of RNase E in cyanobacteria. Nucleic Acids Research. 2024;52(1):404-
931 19. doi: 10.1093/nar/gkad1094.
932 66. Karimova G, Ullmann A, Ladant D. [5] A bacterial two-hybrid system that exploits a cAMP
933 signaling cascade in Escherichia coli. In: Thorner J, Emr SD, Abelson JN, editors. Methods in
934 Enzymology. 328: Academic Press; 2000. p. 59-73.
935 67. Jander G, Rahme Laurence G, Ausubel Frederick M. Positive Correlation between Virulence
936 ofPseudomonas aeruginosa Mutants in Mice and Insects. Journal of Bacteriology. 2000;182(13):3843-
937 5. doi: 10.1128/jb.182.13.3843-3845.2000.
938 68. Lin J, Cheng J, Wang Y, Shen X. The Pseudomonas Quinolone Signal (PQS): Not Just for
939 Quorum Sensing Anymore. Front Cell Infect Microbiol. 2018;8:230. Epub 20180704. doi:
940 10.3389/fcimb.2018.00230. PubMed PMID: 30023354; PubMed Central PMCID: PMCPMC6039570.
941 69. Gonçalves T, Vasconcelos U. Colour Me Blue: The History and the Biotechnological Potential
942 of Pyocyanin. Molecules. 2021;26(4). Epub 20210210. doi: 10.3390/molecules26040927. PubMed
943 PMID: 33578646; PubMed Central PMCID: PMCPMC7916356.
944 70. Chou HT, Li J-Y, Lu C-D. Functional Characterization of the agtABCD and agtSR Operons for
945 4-Aminobutyrate and 5-Aminovalerate Uptake and Regulation in Pseudomonas aeruginosa PAO1.
946 Current Microbiology. 2014;68(1):59-63. doi: 10.1007/s00284-013-0446-y.
947 71. Hauser AR. The type III secretion system of Pseudomonas aeruginosa: infection by injection.
948 Nat Rev Microbiol. 2009;7(9):654-65. doi: 10.1038/nrmicro2199. PubMed PMID: 19680249; PubMed
949 Central PMCID: PMCPMC2766515.
950 72. Nandana V, Al-Husini N, Vaishnav A, Dilrangi KH, Schrader JM. Caulobacter crescentus
951 RNase E condensation contributes to autoregulation and fitness. Mol Biol Cell. 2024;35(8):ar104. Epub
952 20240612. doi: 10.1091/mbc.E23-12-0493. PubMed PMID: 38865176; PubMed Central PMCID:
953 PMCPMC11321048.
954 73. Wurtzel O, Yoder-Himes DR, Han K, Dandekar AA, Edelheit S, Greenberg EP, et al. The single-
955 nucleotide resolution transcriptome of Pseudomonas aeruginosa grown in body temperature. PLoS
956 Pathog. 2012;8(9):e1002945. Epub 20120927. doi: 10.1371/journal.ppat.1002945. PubMed PMID:
957 23028334; PubMed Central PMCID: PMCPMC3460626.
958 74. de Araújo Hugo L, Picinato Beatriz A, Lorenzetti Alan PR, Muthunayake Nisansala S,
959 Rathnayaka-Mudiyanselage IW, dos Santos Naara M, et al. The DEAD-box RNA helicase RhlB is
960 required for efficient RNA processing at low temperature in Caulobacter. Microbiology Spectrum.
961 2023;11(6):e01934-23. doi: 10.1128/spectrum.01934-23.
962 75. Vaillancourt M, Galdino ACM, Limsuwannarot SP, Celedonio D, Dimitrova E, Broerman M,
963 et al. A compensatory RNase E variation increases Iron Piracy and Virulence in multidrug-resistant
964 *Pseudomonas aeruginosa* during Macrophage infection. PLoS Pathog. 2023;19(4):e1010942. Epub

965 20230407. doi: 10.1371/journal.ppat.1010942. PubMed PMID: 37027441; PubMed Central PMCID:
966 PMCPMC10115287.
967 76. Khemici V, Toesca I, Poljak L, Vanzo NF, Carpousis AJ. The RNase E of *Escherichia coli* has
968 at least two binding sites for DEAD-box RNA helicases: functional replacement of RhlB by RhlE.
969 Molecular Microbiology. 2004;54(5):1422-30. doi: https://doi.org/10.1111/j.1365-2958.2004.04361.x.
970 77. Worrall JA, Howe FS, McKay AR, Robinson CV, Luisi BF. Allosteric activation of the ATPase
971 activity of the *Escherichia coli* RhlB RNA helicase. J Biol Chem. 2008;283(9):5567-76. PubMed
972 PMID: 18165229.
973 78. Lüthi E, Mercenier A, Haas D. The arcABC Operon Required for Fermentative Growth of
974 Pseudomonas aeruginosa on Arginine: Tn5-751-assisted Cloning and Localization of Structural Genes.
975 Microbiology. 1986;132(10):2667-75. doi: https://doi.org/10.1099/00221287-132-10-2667.
976 79. Gamper M, Ganter B, Polito MR, Haas D. RNA processing modulates the expression of the
977 *arcDABC* operon in *Pseudomonas aeruginosa*. Journal of Molecular Biology. 1992;226(4):943-57. doi:
978 https://doi.org/10.1016/0022-2836(92)91044-P.
979 80. Rietsch A, Vallet-Gely I, Dove SL, Mekalanos JJ. ExsE, a secreted regulator of type III
980 secretion genes in Pseudomonas aeruginosa. Proc Natl Acad Sci U S A. 2005;102(22):8006-11. Epub
981 20050523. doi: 10.1073/pnas.0503005102. PubMed PMID: 15911752; PubMed Central PMCID:
982 PMCPMC1142391.
983 81. Laville J, Voisard C, Keel C, Maurhofer M, Défago G, Haas D. Global control in Pseudomonas
984 fluorescens mediating antibiotic synthesis and suppression of black root rot of tobacco. Proc Natl Acad
985 Sci U S A. 1992;89(5):1562-6. doi: 10.1073/pnas.89.5.1562. PubMed PMID: 1311842; PubMed Central
986 PMCID: PMCPMC48492.
987 82. Ye RW, Haas D, Ka JO, Krishnapillai V, Zimmermann A, Baird C, Tiedje JM. Anaerobic
988 activation of the entire denitrification pathway in Pseudomonas aeruginosa requires Anr, an analog of
989 Fnr. J Bacteriol. 1995;177(12):3606-9. doi: 10.1128/jb.177.12.3606-3609.1995. PubMed PMID:
990 7768875; PubMed Central PMCID: PMCPMC177071.
991 83. Bordi C, Lamy MC, Ventre I, Termine E, Hachani A, Fillet S, et al. Regulatory RNAs and the
992 HptB/RetS signalling pathways fine-tune Pseudomonas aeruginosa pathogenesis. Mol Microbiol.
993 2010;76(6):1427-43. Epub 20100401. doi: 10.1111/j.1365-2958.2010.07146.x. PubMed PMID:
994 20398205; PubMed Central PMCID: PMCPMC2904497.
995 84. Schindelin J, Arganda-Carreras I, Frise E, Kaynig V, Longair M, Pietzsch T, et al. Fiji: an open-
996 source platform for biological-image analysis. Nat Methods. 2012;9(7):676-82. Epub 20120628. doi:
997 10.1038/nmeth.2019. PubMed PMID: 22743772; PubMed Central PMCID: PMCPMC3855844.
998 85. Team RC. R: A Language and Environment for Statistical Computing. R Foundation for
999 Statistical Computing. Vienna, Austria2023.

86. Ream JA, Lewis LK, Lewis KA. Rapid agarose gel electrophoretic mobility shift assay for quantitating protein: RNA interactions. Anal Biochem. 2016;511:36-41. Epub 20160802. doi: 10.1016/j.ab.2016.07.027. PubMed PMID: 27495142; PubMed Central PMCID: PMCPMC5002362.

87. Langmead B, Salzberg SL. Fast gapped-read alignment with Bowtie 2. Nature Methods. 2012;9(4):357-9. doi: 10.1038/nmeth.1923.

88. Lawrence M, Huber W, Pagès H, Aboyoun P, Carlson M, Gentleman R, et al. Software for Computing and Annotating Genomic Ranges. PLOS Computational Biology. 2013;9(8):e1003118. doi: 10.1371/journal.pcbi.1003118.

89. Love MI, Huber W, Anders S. Moderated estimation of fold change and dispersion for RNA-seq data with DESeq2. Genome Biology. 2014;15(12):550. doi: 10.1186/s13059-014-0550-8.

90. B. TDM. KEGGREST: Client-side REST access to the Kyoto Encyclopedia of Genes and Genomes (KEGG). doi:10.18129/B9.bioc.KEGGREST. R package version 1420, https://bioconductororg/packages/KEGGREST2023.

91. de Araújo HL, Picinato BA, Lorenzetti APR, Muthunayake NS, Rathnayaka-Mudiyanselage IW, Dos Santos NM, et al. The DEAD-box RNA helicase RhlB is required for efficient RNA processing at low temperature in Caulobacter. Microbiol Spectr. 2023:e0193423. Epub 2023/10/18. doi: 10.1128/spectrum.01934-23. PubMed PMID: 37850787.

92. Altschul SF, Gish W, Miller W, Myers EW, Lipman DJ. Basic local alignment search tool. J Mol Biol. 1990;215(3):403-10. doi: 10.1016/s0022-2836(05)80360-2. PubMed PMID: 2231712.

93. Pagès HA, P.; Gentleman, R.; DebRoy, S. Biostrings: Efficient manipulation of biological strings. 2024.

94. Grant BJ, Rodrigues AP, ElSawy KM, McCammon JA, Caves LS. Bio3d: an R package for the comparative analysis of protein structures. Bioinformatics. 2006;22(21):2695-6. Epub 20060829. doi: 10.1093/bioinformatics/btl461. PubMed PMID: 16940322.

95. Edgar RC. MUSCLE: multiple sequence alignment with high accuracy and high throughput. Nucleic Acids Res. 2004;32(5):1792-7. Epub 20040319. doi: 10.1093/nar/gkh340. PubMed PMID: 15034147; PubMed Central PMCID: PMCPMC390337.

96. Erdős G, Pajkos M, Dosztányi Z. IUPred3: prediction of protein disorder enhanced with unambiguous experimental annotation and visualization of evolutionary conservation. Nucleic Acids Research. 2021;49(W1):W297-W303. doi: 10.1093/nar/gkab408.

97. Xue B, Dunbrack RL, Williams RW, Dunker AK, Uversky VN. PONDR-FIT: a meta-predictor of intrinsically disordered amino acids. Biochim Biophys Acta. 2010;1804(4):996-1010. Epub 20100125. doi: 10.1016/j.bbapap.2010.01.011. PubMed PMID: 20100603; PubMed Central PMCID: PMCPMC2882806.

98. McLaren RS, Newbury SF, Dance GS, Causton HC, Higgins CF. mRNA degradation by processive 3'-5' exoribonucleases in vitro and the implications for prokaryotic mRNA decay in vivo. J Mol Biol. 1991;221(1):81-95. PubMed PMID: 1920421.

1037 99. Bolte S, Cordelières FP. A guided tour into subcellular colocalization analysis in light
1038 microscopy. J Microsc. 2006;224(Pt 3):213-32. doi: 10.1111/j.1365-2818.2006.01706.x. PubMed
1039 PMID: 17210054.

1040

1041 **Figure Legends**

1042

1043 **Figure 1: Comparison of *E. coli* (Ec) and *P. aeruginosa* (Pa) RNase E architecture. (A)** Ec RNase
1044 E architecture, adapted from [17]. The NTD is shown is grey, and experimentally defined regions
1045 necessary for interaction with the membrane, with RNA, or with the three core protein partners are
1046 highlighted in red, dark blue, and yellow/purple/pink, respectively. **(B)** Pa RNase E architecture based
1047 on in-silico analyses performed in Fig S1-S2 and in [59]. The SLiM nomenclature was taken from [59],
1048 while the consensus sequence characterising each SLiM was specifically adapted based on sequence
1049 conservation within the Pseudomonas genus (Fig S1). MTS: membrane-targeting sequence, AR4:
1050 arginine-rich motif 4, REER-repeats: region with high frequency of occurrence of "RE[E/D]R" motif,
1051 M29: motif 29, AR1: arginine-rich motif 1, M20: motif 20, NDPR: motif with a highly conserved NDPR
1052 sequence. All diagrams were drawn to scale. IUPRED3 [96] and PONDR [97] predictions of disorder
1053 propensity (probability score) are shown for Ec RNase E **(A)** and Pa RNase E **(B)**.

1054

1055 **Figure 2: RNA binding of Pa RNase E CTD via the AR1, AR4, and REER SLiMs. (A)** EMSA with
1056 purified His-Smt3 tagged RNase E CTD$^{572-1057}$ variants having either the native sequence (WT) or
1057 systematic alanine mutation of the arginine residues found within the REER-repeats region (REERmut),
1058 the AR4 SLiM (AR4mut) or the AR1 SLiM (AR1mut). The *malEF* mRNA intergenic region was used
1059 as a substrate [98]. Ratios of RNA:protein ranging from 1:10 to 1:80 were tested. See Fig S2 for
1060 additional EMSA with additional RNA:protein ratios. **(B)** Representative microscopy images of a PAO1
1061 strain expressing the RNase E-msfGFP fusion or mutated or truncated variants as indicated. **(C)**
1062 Quantification of signal intensity variance in the strains of panel B as indication of foci disappearance
1063 (see methods). **(D)** Representative microscopy images of a PAO1 strain expressing the RNase E-
1064 msfGFP fusion after exposure to rifampicin (+ Rif, exposure to a concentration of 100 µg/mL for 30
1065 minutes) or to DMSO as a negative control (- Rif). Corrected mean fluorescent signal intensity **(E)** and
1066 signal intensity variance **(F)** is showed in the graphs (see methods). Each quantification analysis
1067 involved at least 50 individual cells. The scale is 2 µm. Statistical significance was assessed by
1068 performing t-tests using R. p-values for comparisons tested are indicated as follows: *:<0.05; **:<0.01;
1069 ***:<0.001; ****:<0.0001.

1070

1071 **Figure 3**: **Identification of scaffold domain-dependent RNase E protein partners by pull-down**
1072 **assays and mapping of the interactions by bacterial two-hybrid assays (A)** Volcano plot
1073 highlighting the relative enrichment of proteins co-eluting with the RNase E$^{1-1057}$-Strep bait protein
1074 compared to the untagged negative control. The plot was generated from the average peptide count
1075 obtained in duplicate pull-down experiments. An arbitrary threshold of 5.5-fold change was chosen for
1076 selection of candidate (c) proteins. **(B)** Scatterplot highlighting comparative enrichment of proteins co-
1077 eluting with the RNase E$^{1-1057}$-Strep bait protein (x axis) or with the RNase E$^{1-529}$-Strep bait protein (y

axis) compared to the untagged negative control. **(C)** Quantification of β-galactosidase activity in *E. coli* BTH101 cells co-expressing T18-RNase E with T25-PNPase, T25-RhlB, T25-ArcB, T25-GdhB or T25-RpoB. Interaction between T18-RNase E and a T25-tagged protein partner results in a significant restoration of β-galactosidase activity compared with empty vector (e.v.) negative controls. Unpaired Welch's t-tests was performed using GraphPad Prism to assess differences between every tested protein-protein interaction and the respective negative control. ***: p-value <0.0001; n.s: not significant (99% confidence level). **(D-F)** Mapping of the interaction between RNase E and PNPase **(D)**, RhlB **(E)**, or ArcB **(F)** by quantification of β-galactosidase activity in *E. coli* BTH101 cells co-expressing T25-PNPase **(D)**, T25-RhlB **(E)**, or T25-ArcB **(F)** and either T18-RNase E or one of eight to ten truncated T18-RNase E fragments. Empty vector (e.v.) negative controls are included into each separate graph for comparison.

Figure 4: PNPase and RhlB directly interact with RNase E scaffold domain via NDPR and AR1 SLiMs, respectively. Purified Flag-tagged RNase E^{1-529} or RNase $E^{572-1057}$ proteins having either native or mutated sequence were used as baits, immobilized to anti-flag magnetic beads and incubated with purified His-Smt3 tagged PNPase **(A)** or RhlB **(B)** proteins to assess direct protein binding. I: input, F: free fraction, B: bound fraction. NDPRmut, AR1mut: mutations of NDPR and AR1 SLiMs, respectively (see Table S4). Binding assays were repeated at least 3-times and representative gels are shown.

Figure 5: **Colocalisation of PNPase or RhlB with RNase E foci is dependent on their interaction with NDPR and AR1 RNase E SLiMs, respectively. (A)** Visualisation of PNPase-msfGFP (upper panels) or RhlB-msfGFP (lower panels) fusion and RNase E-mCherry fusion co-expressed in the same strain. Pearson's and M coefficients were calculated in Fiji using the JaCoP plugin [99]. Three independent images were used, each containing at least 30 cells, and an average coefficient was calculated from the three values obtained with each image. **(B)** Visualisation of PNPase-msfGFP (upper panels) and RhlB-msfGFP (lower panels) in strains expressing either the native RNase E protein (full length) or truncated variants, as indicated above each image. Scale is 2 µm.

Figure 6: Phenotypes affected by deletion or mutation of RNase E scaffolding domain. (A) Growth on NA agar plates at 37°C or 16°C, or under low vs high pH conditions of wild-type (WT), *rne588*, *rne529*, *rne*AR1^{mut}, *rne*NDPR^{mut}, and *rne*AR1+AR4+REER^{mut} strains, as indicated. Experiments were performed in biological independent triplicates; a representative plate is shown. **(B)** Growth in NYB broth at 37°C in 96-well plates of wild-type (WT), *rne588*, *rne529*, *rne*AR1^{mut}, *rne*NDPR^{mut}, and *rne*AR1+AR4+REER^{mut} strains, as indicated. Independent biological triplicates, each with four technical replicates, were used to generate the average growth curve shown. **(C)** Killing curves of *G. mellonella* larvae injected with 10 µL of WT or mutant *P. aeruginosa* strains (as in panel A). The control group was injected with 10 µL of sterile PBS instead. Larvae were incubated at 37°C and larval death

1115 was monitored over 13-26 hours post-injection. A larva was considered dead when it completely
1116 stopped responding to repeated touching stimuli. Two independent replicates were performed using a
1117 total of at least 50 larvae for each strain tested. A Kaplan-Meier test for survival analysis was performed
1118 using GraphPad Prism and comparing the survival curve of each mutant strain to that of the WT strain.
1119 ***: p-value <0.0001; n.s: not significant (99% confidence interval).
1120

1121 **Figure 7: RNA-seq analysis of RNase E CTD truncated mutants reveals broad transcriptome**
1122 **changes. (A-B)** Volcano plots highlighting genes differentially regulated in the **(A)** *rne*$^{1-529}$ (R529) or
1123 **(B)** *rne* $^{1-588}$ (R588) mutant strains compared with the WT strain. Genes significantly up- or down-
1124 regulated (P-value < 0.05, fold change |FC| ≥ 2) are highlighted in red or blue, respectively. **(C)**
1125 Scatterplot of genes differentially regulated in *rne* $^{1-529}$ strain versus genes differentially regulated in
1126 *rne*$^{1-588}$ strain, highlighting commonalities and differences between the two mutant strains. **(D-E)**
1127 Clustered heat maps of type 3 secretion system **(D)** or ribosomal proteins **(E)** transcript levels in the
1128 RNase E$^{1-529}$ and by about 2-fold in the RNase E$^{1-588}$ strains as compared to the WT strain (fold change).
1129 **(F)** Differential analyses (log 2-fold change) of normalized total reads counts corresponding to the 5'
1130 UTR region of the PA2976 (*rne*) transcript or RNase E NTD coding sequence in the RNase E$^{1-529}$ and
1131 by about 2-fold in the RNase E$^{1-588}$ strains as compared to the WT strain. **(G)** Proportion of loci with 5'
1132 read ends (sequenced fragments) counted only in a strain (nominator) relative to the 5' read ends counted
1133 in that strain and in a WT replica (denominator). A total of 8 million reads was analysed in each strain
1134 to exclude an effect due to the library depth (see methods). Histograms of individual values calculated
1135 per each strain and replicate is shown in Figure S8.
1136

1137 **Figure 8: Model of RNA degradosome in *P. aeruginosa*.** Numbers corresponds to RNase E SLiM
1138 start-end residues involved in membrane, RNA, RhlB or PNPase interaction. RNA is represented as a
1139 dotted line. See discussion for details.

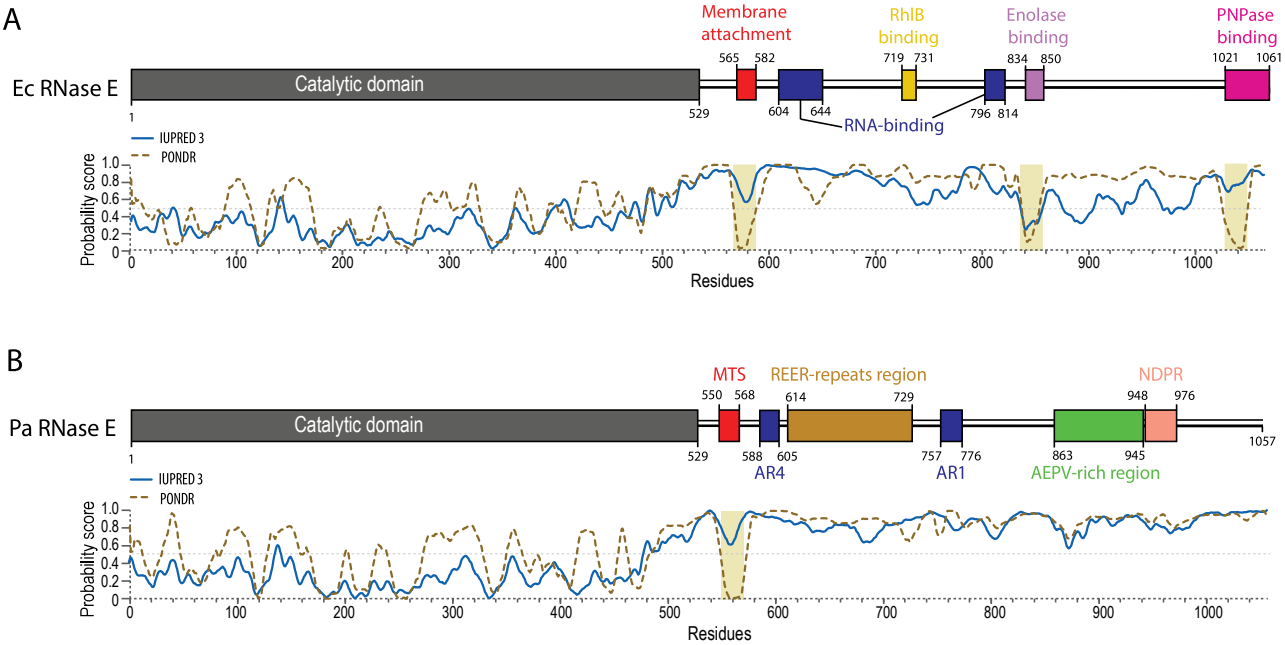
A
Ec RNase E
Catalytic domain
Membrane attachment
RhlB binding
Enolase binding
PNPase binding
565 582
719 731
834 850
1021 1061
1
529
604 644
796 814
RNA-binding
IUPRED 3
PONDR
Probability score
Residues
B
Pa RNase E
Catalytic domain
MTS
REER-repeats region
NDPR
550 568
614
729
948 976
1057
529
588 605
757 776
863 945
AR4
AR1
AEPV-rich region
IUPRED 3
PONDR
Probability score
Residues

Figure 1

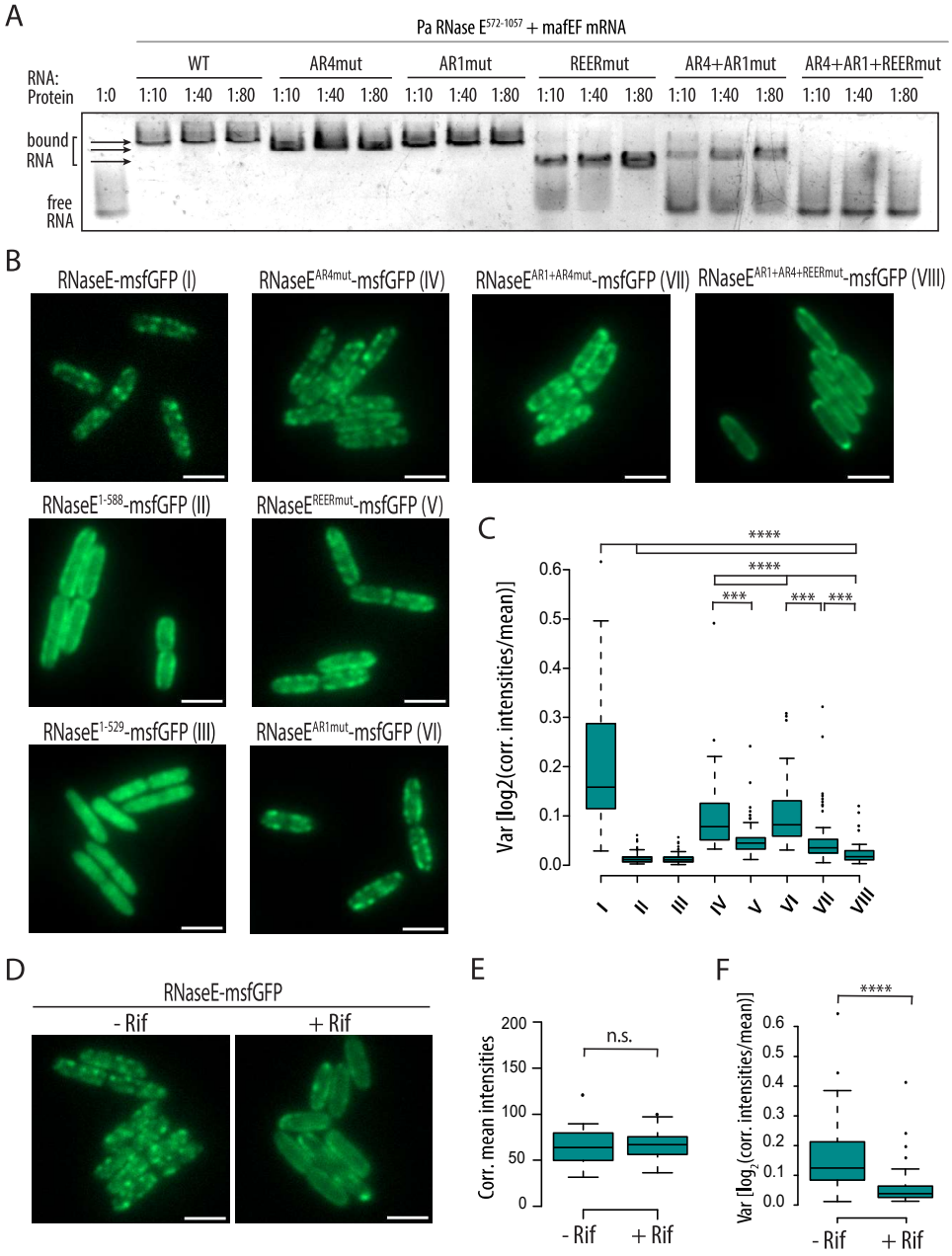
A
Pa RNase E572-1057 + mafEF mRNA
WT
AR4mut
AR1mut
REERmut
AR4+AR1mut
AR4+AR1+REERmut
RNA:
Protein
1:0
1:10
1:40
1:80
bound RNA
free RNA
B
RNaseE-msfGFP (I)
RNaseEAR4mut-msfGFP (IV)
RNaseEAR1+AR4mut-msfGFP (VII)
RNaseEAR1+AR4+REERmut-msfGFP (VIII)
RNaseE1-588-msfGFP (II)
RNaseEREERmut-msfGFP (V)
RNaseE1-529-msfGFP (III)
RNaseEAR1mut-msfGFP (VI)
C
Var [log2(corr. intensities/mean)]
****
***
I
II
III
IV
V
VI
VII
VIII
D
RNaseE-msfGFP
- Rif
+ Rif
E
Corr. mean intensities
n.s.
F
Var [log2(corr. intensities/mean)]

Figure 2

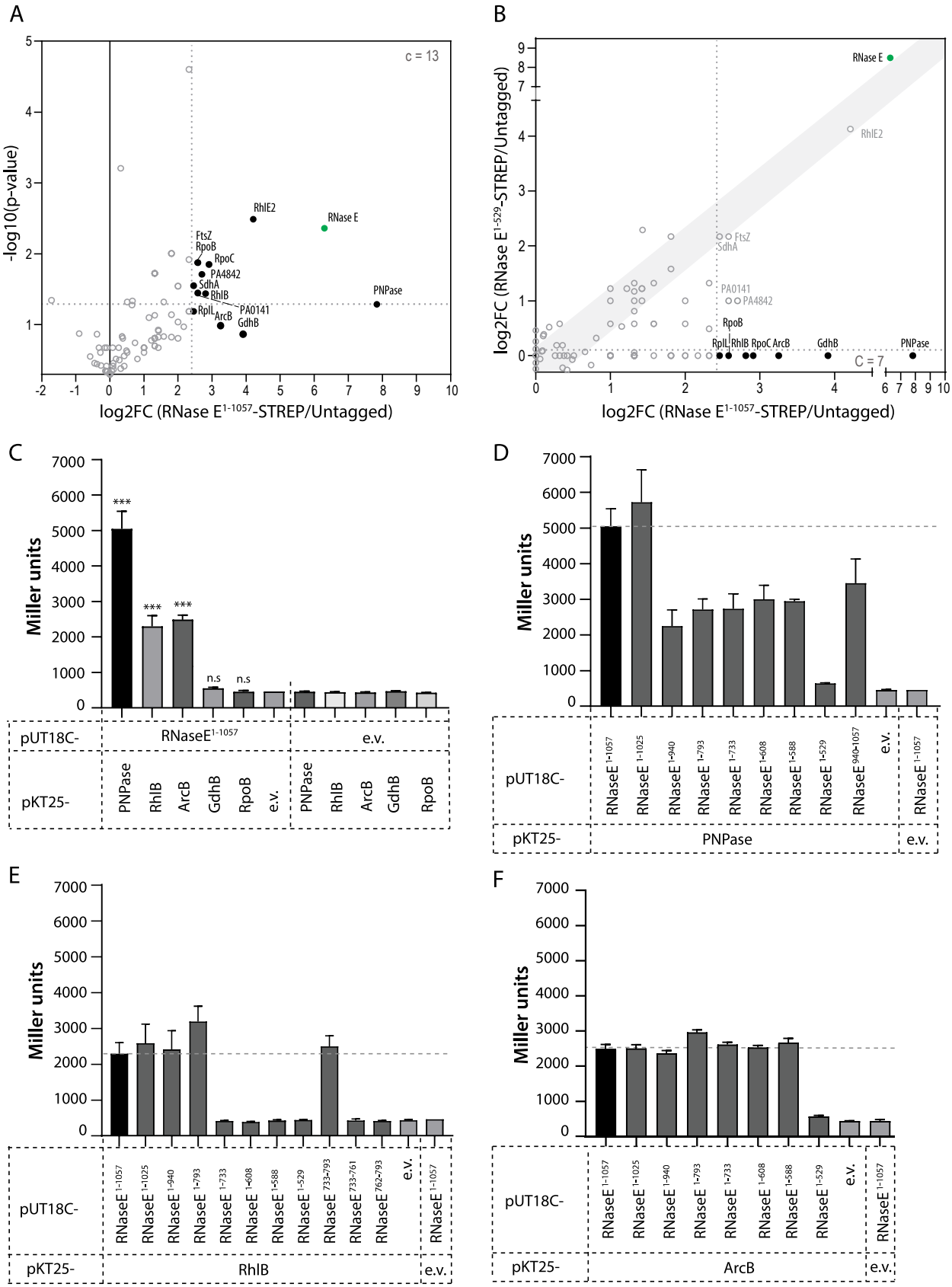
A
c = 13
-log10(p-value)
log2FC (RNase E1-1057-STREP/Untagged)
RhlE2
RNase E
FtsZ
RpoB
RpoC
PA4842
SdhA
RhlB
RplL
PA0141
ArcB
GdhB
PNPase
B
RNase E
RhlE2
FtsZ
SdhA
PA0141
PA4842
RpoB
RplL
RhlB
RpoC
ArcB
GdhB
PNPase
C = 7
log2FC (RNase E1-529-STREP/Untagged)
log2FC (RNase E1-1057-STREP/Untagged)
C
Miller units
***
n.s
pUT18C-
RNaseE1-1057
e.v.
pKT25-
PNPase
RhlB
ArcB
GdhB
RpoB
e.v.
D
Miller units
pUT18C-
RNaseE1-1057
RNaseE1-1025
RNaseE1-940
RNaseE1-793
RNaseE1-733
RNaseE1-608
RNaseE1-588
RNaseE1-529
RNaseE940-1057
e.v.
pKT25-
PNPase
e.v.
E
Miller units
pUT18C-
RNaseE1-1057
RNaseE1-1025
RNaseE1-940
RNaseE1-793
RNaseE1-733
RNaseE1-608
RNaseE1-588
RNaseE1-529
RNaseE733-793
RNaseE733-761
RNaseE762-793
e.v.
pKT25-
RhlB
e.v.
F
Miller units
pUT18C-
RNaseE1-1057
RNaseE1-1025
RNaseE1-940
RNaseE1-793
RNaseE1-733
RNaseE1-608
RNaseE1-588
RNaseE1-529
e.v.
pKT25-
ArcB
e.v.

Figure 3

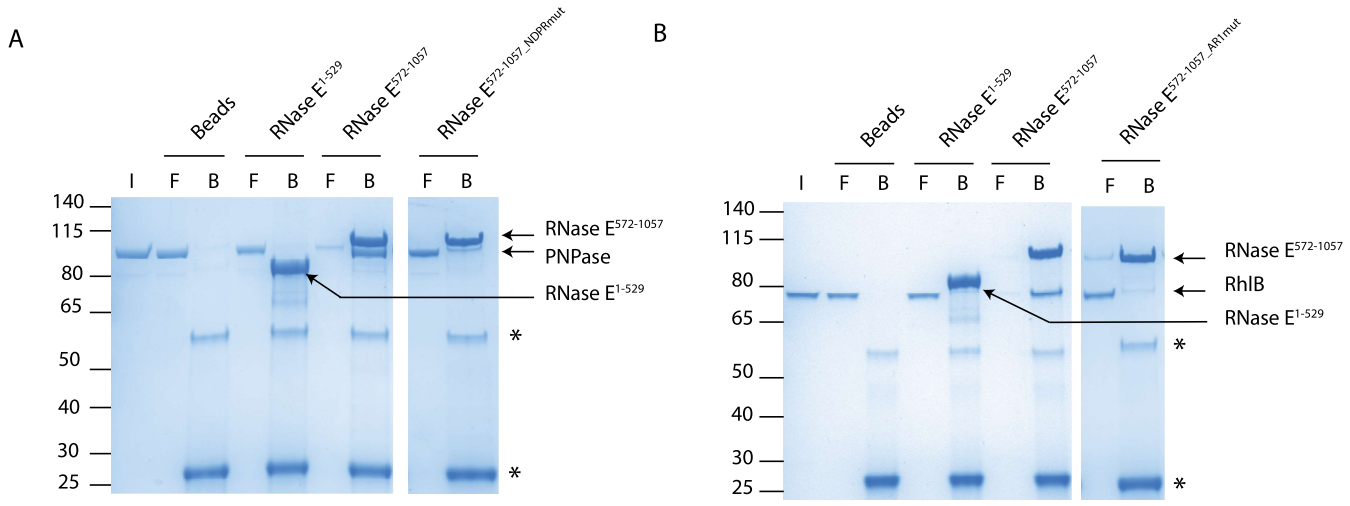
A
Beads
RNase E1-529
RNase E572-1057
RNase E572-1057_NDPRmut
I F B F B F B F B
140
115
80
65
50
40
30
25
RNase E572-1057
PNPase
RNase E1-529
*
*
B
Beads
RNase E1-529
RNase E572-1057
RNase E572-1057_AR1mut
I F B F B F B F B
140
115
80
65
50
40
30
25
RNase E572-1057
RhlB
RNase E1-529
*
*

Figure 4

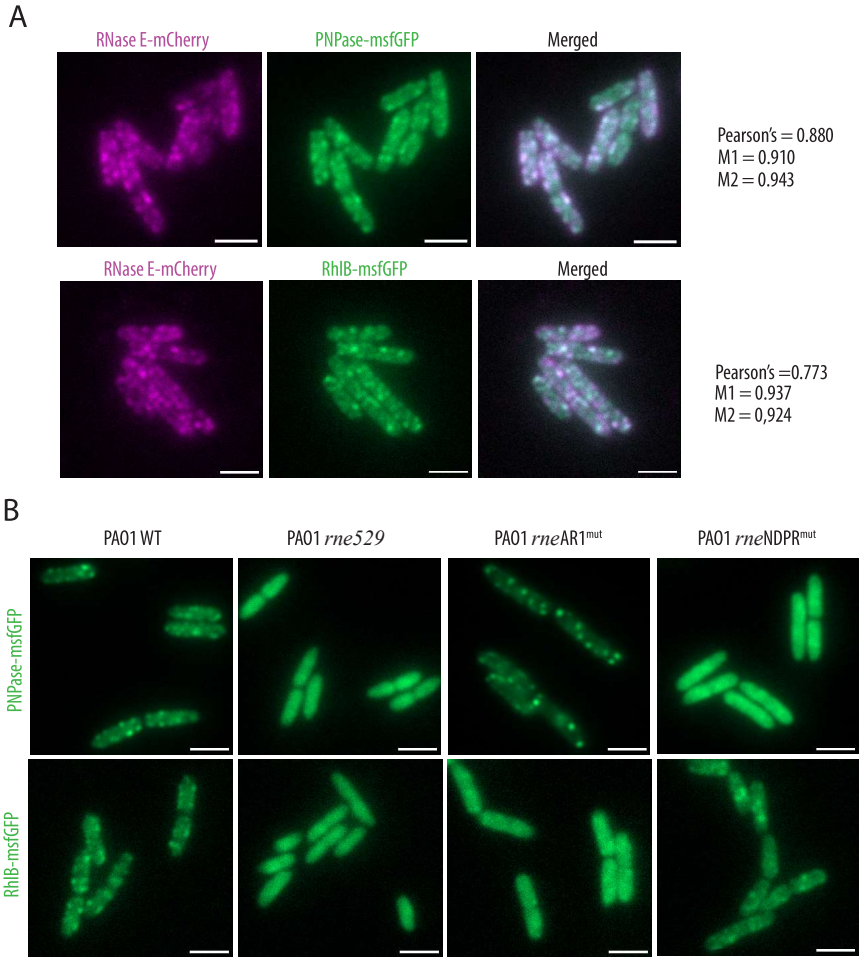
A
RNase E-mCherry
PNPase-msfGFP
Merged
Pearson's = 0.880
M1 = 0.910
M2 = 0.943
RNase E-mCherry
RhlB-msfGFP
Merged
Pearson's =0.773
M1 = 0.937
M2 = 0,924
B
PAO1 WT
PAO1 rne529
PAO1 rneAR1mut
PAO1 rneNDPRmut
PNPase-msfGFP
RhlB-msfGFP

Figure 5

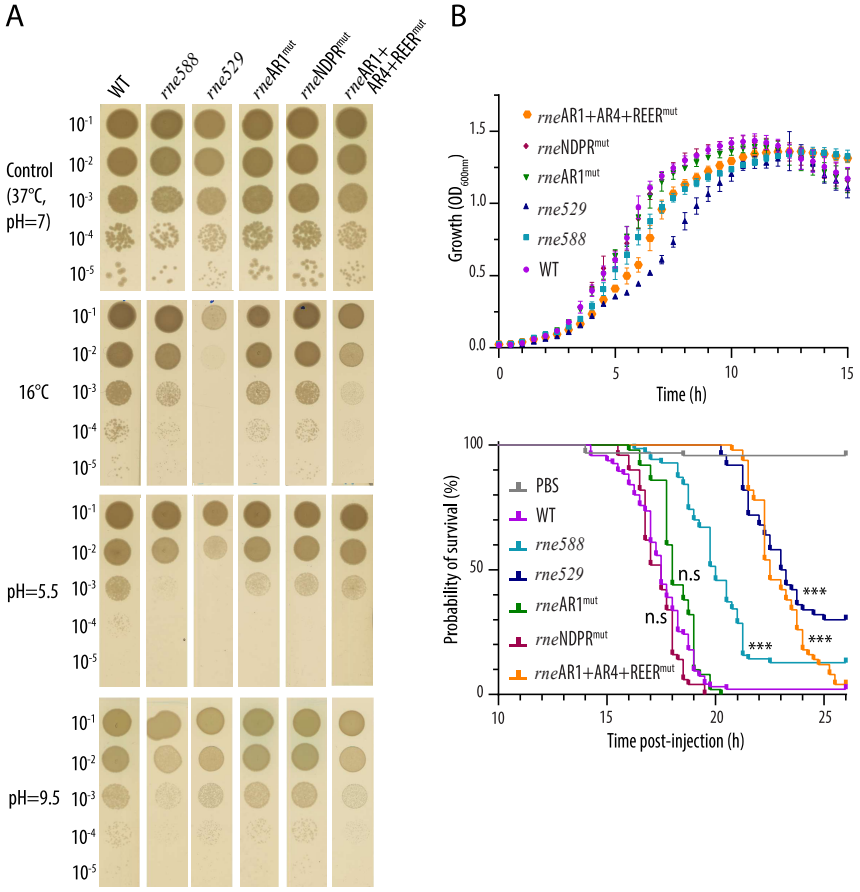
A
WT
rne588
rne529
rneAR1mut
rneNDPRmut
rneAR1+ AR4+REERmut
Control (37°C, pH=7)
16°C
pH=5.5
pH=9.5
10-1
10-2
10-3
10-4
10-5
B
rneAR1+AR4+REERmut
rneNDPRmut
rneAR1mut
rne529
rne588
WT
Growth (OD600nm)
Time (h)
PBS
WT
rne588
rne529
rneAR1mut
rneNDPRmut
rneAR1+AR4+REERmut
n.s
n.s
***
***
***
Probability of survival (%)
Time post-injection (h)

Figure 6

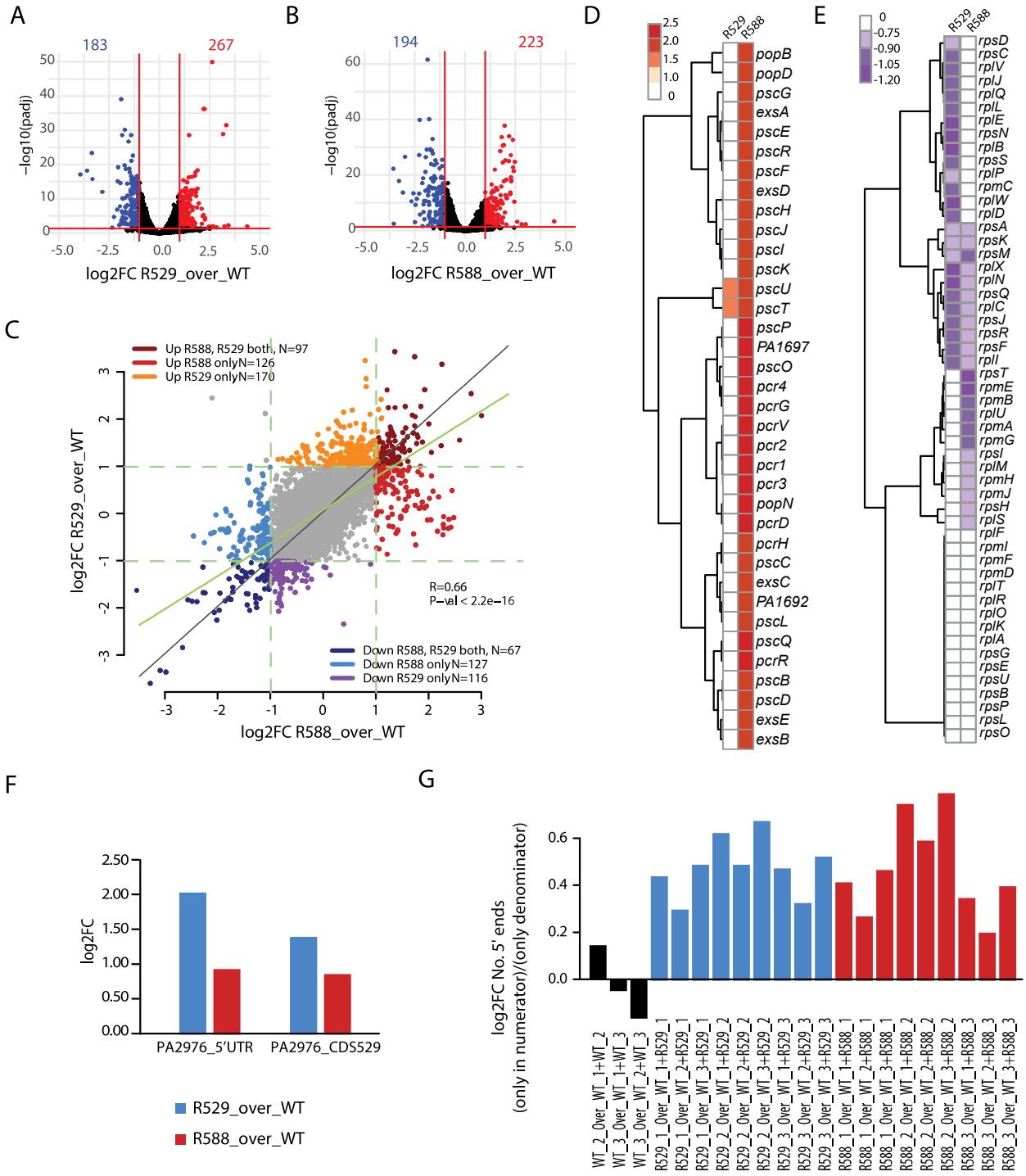
A
183
267
−log10(padj)
log2FC R529_over_WT
B
194
223
−log10(padj)
log2FC R588_over_WT
C
Up R588, R529 both, N=97
Up R588 only N=126
Up R529 only N=170
R=0.66
P−val < 2.2e−16
Down R588, R529 both, N=67
Down R588 only N=127
Down R529 only N=116
log2FC R529_over_WT
log2FC R588_over_WT
D
R529
R588
popB
popD
pscG
exsA
pscE
pscR
pscF
exsD
pscH
pscJ
pscI
pscK
pscU
pscT
pscP
PA1697
pscO
pcr4
pcrG
pcrV
pcr2
pcr1
pcr3
popN
pcrD
pcrH
pscC
exsC
PA1692
pscL
pscQ
pcrR
pscB
pscD
exsE
exsB
E
R529
R588
rpsD
rpsC
rplV
rplJ
rplQ
rplL
rplE
rpsN
rplB
rpsS
rplP
rpmC
rplW
rplD
rpsA
rpsK
rpsM
rplX
rplN
rpsQ
rplC
rpsJ
rpsR
rpsF
rplI
rpsT
rpmE
rpmB
rplU
rpmA
rpmG
rpsI
rplM
rpmH
rpmJ
rpsH
rplS
rplF
rpmI
rpmF
rpmD
rplT
rplR
rplO
rplK
rplA
rpsG
rpsE
rpsU
rpsB
rpsP
rpsL
rpsO
F
log2FC
PA2976_5'UTR
PA2976_CDS529
R529_over_WT
R588_over_WT
G
log2FC No. 5' ends
(only in numerator)/(only denominator)
WT_2_Over_WT_1+WT_2
WT_3_Over_WT_1+WT_3
WT_3_Over_WT_2+WT_3
R529_1_Over_WT_1+R529_1
R529_1_Over_WT_2+R529_1
R529_1_Over_WT_3+R529_1
R529_2_Over_WT_1+R529_2
R529_2_Over_WT_2+R529_2
R529_2_Over_WT_3+R529_2
R529_3_Over_WT_1+R529_3
R529_3_Over_WT_2+R529_3
R529_3_Over_WT_3+R529_3
R588_1_Over_WT_1+R588_1
R588_1_Over_WT_2+R588_1
R588_1_Over_WT_3+R588_1
R588_2_Over_WT_1+R588_2
R588_2_Over_WT_2+R588_2
R588_2_Over_WT_3+R588_2
R588_3_Over_WT_1+R588_3
R588_3_Over_WT_2+R588_3
R588_3_Over_WT_3+R588_3

Figure 7

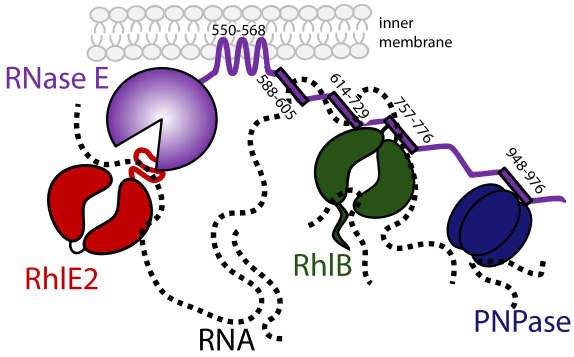
inner
membrane
550-568
RNase E
588-605
614-729
757-776
948-976
RhlE2
RhlB
RNA
PNPase

Figure 8